A Unifying Passivity-Based Framework for Pressure and Volume Flow Rate Control in District Heating Networks

Felix Strehle, Juan E. Machado, Michele Cucuzzella, *Member, IEEE*, Albertus Johannes Malan, Sören Hohmann, *Member, IEEE*, and Jacquelien M. A. Scherpen, *Fellow, IEEE*

***Abstract*— A fundamental precondition for the operation of district heating networks (DHNs) is a stable hydraulic behavior. However, the ongoing transition toward a sustainable heat supply, especially the rising integration of distributed heat sources and the increasingly meshed topologies, introduces complex and potentially destabilizing hydraulic dynamics. In this work, we propose a unifying, equilibrium-independent passivity (EIP)-based control framework, which guarantees asymptotic stability of any feasible, hydraulic DHN equilibrium for a wide range of DHN setups covering different DHN generations, meshed, time-varying topologies, and multiple, dynamically interacting distributed heat sources. The obtained results hold for the state of the art as well as future DHN generations featuring, for example, multiple distributed heat sources, asymmetric pipe networks, and multiple temperature layers.**

***Index Terms*— Decentralized control, fluid flow control, hydraulic systems, nonlinear control systems, pressure control, stability analysis.**

I. Introduction

DISTRICT heating networks (DHNs) are a key element for a holistic energy transition, particularly in densely populated areas [2], [3], [4], [5]. For their operation, well-defined and stable hydraulic conditions are a fundamental requirement, as they form the basis for the actual thermal power flows [4], [6]. In traditional second- or third-generation DHNs, the hydraulics and, thus, the thermal power flows are well understood (see [7, pp. 52–54]). However, emerging fourth-generation DHNs bring about challenges that call for new strategies and methods of operating, controlling, and analyzing DHNs [2], [3], [4], [8].[1] Most prominently, we can observe a *decentralization* trend with several interacting subsystems and controllable components, such as distributed variable speed pumps (DVSPs) and control valves. Primarily, this is due to the desire of flexibly and efficiently integrating ever more renewable and distributed heat generation units (DGUs), e.g., heat pumps, combined heat and power, or solar thermal power plants [2], [3], [5], [9], [10]. Furthermore, the integration of—typically intermittent—renewable heat sources and new types of consumers, such as low-energy buildings, is supported by novel, more efficient DHN setups that have multiple temperature layers and in which more frequent changes in the hydraulic conditions occur [2], [3], [11], [12], [13]. To ensure a proper heat supply in such new DHN setups, it is required to include additional controllable devices, such as booster pumps, at strategic points in the DHN, e.g., in crucial pipes or at consumers [2], [7, p. 54], [14]. However, this leads to complex pressure and volume flow dynamics and interactions on small time scales [4], which may produce more frequent volume flow reversals in pipes [15], [16] or severe hydraulic oscillations [5], [9], [17].

To face the abovementioned challenges and ensure stable hydraulic conditions, we present a unifying framework based on equilibrium-independent passivity (EIP) for the *decentralized* pressure and volume flow rate control in general DHN setups. In summary, our main contributions are as follows.

A. C1

Using a graph-theoretic approach, we modularly derive a comprehensive control design model covering the hydraulic dynamics of general DHNs with an arbitrary number of DGUs and consumers that are connected in a meshed, possibly asymmetric pipe network topology with multiple temperature layers. In particular, our model encompasses traditional second- and third-generation DHNs, future fourth-generation

[1] See [2] for a comparison and overview of the different DHN generations.

Manuscript received 6 December 2023; accepted 2 February 2024. Date of publication 21 February 2024; date of current version 25 June 2024. This work was supported in part by the Dutch Research Council (NWO) under Grant ESI.2019.005; in part by the NWO, ERA-Net Smart Energy Systems and European Union's Horizon 2020 Research and Innovation Programme under Grant 775970; in part by the German Federal Government; in part by the Federal Ministry of Education and Research; and in part by the State of Brandenburg within the framework of the joint project Energy Innovation Center (EIZ) under Project 85056897 and Project 03SF0693A. Recommended by Associate Editor T. Yang. *(Felix Strehle and Juan E. Machado contributed equally to this work.) (Corresponding author: Michele Cucuzzella.)*

Felix Strehle, Albertus Johannes Malan, and Sören Hohmann are with the Institute of Control Systems, Karlsruhe Institute of Technology (KIT), 76131 Karlsruhe, Germany (e-mail: felix.strehle@kit.edu; albertus.malan@kit.edu; soeren.hohmann@kit.edu).

Juan E. Machado is with the Faculty of Mechanical Engineering, Electrical and Energy Systems, Brandenburg University of Technology, 03046 Cottbus, Germany (e-mail: machadom@b-tu.de).

Michele Cucuzzella is with the Department of Electrical, Computer and Biomedical Engineering, University of Pavia, 27100 Pavia, Italy, and also with the Jan C. Willems Center for Systems and Control, Engineering and Technology Institute Groningen (ENTEG), Faculty of Science and Engineering, University of Groningen, 9747 AG Groningen, The Netherlands (e-mail: michele.cucuzzella@unipv.it).

Jacquelien M. A. Scherpen is with the Jan C. Willems Center for Systems and Control, Engineering and Technology Institute Groningen (ENTEG), Faculty of Science and Engineering, University of Groningen, 9747 AG Groningen, The Netherlands (e-mail: j.m.a.scherpen@rug.nl).

Digital Object Identifier 10.1109/TCST.2024.3365250

DHNs, and intermediate stages. Moreover, we incorporate dynamic models for the pumps, consider valves as actuators, and explicitly account for the presence of pressure holding units. The main challenge behind this contribution was to combine the scattered information from the interdisciplinary literature (e.g., on multitemperature topologies and pressure holding units) and finally translate all into a comprehensive dynamic DHN model suitable for control design and system analysis.

B. C2

We propose decentralized, passivity-based pump and valve controllers for achieving pressure and volume flow rate regulation in the actuated DHN subsystems and ensuring that the closed-loop subsystems are EIP. The pump pressure controller is based on an algebraic interconnection and damping assignment (IDA) [18] extended with integral action on the nonpassive output [19]; the pump volume flow rate controller comprises a state feedback with integral action on the passive output, and the valve volume flow rate controller uses a proportional–integral (PI) action on a modified passive output inspired by Monshizadeh et al. [20]. The main challenge behind this contribution was to deal with the nonlinear, uncertain, and networked nature of the DHN subsystems.

C. C3

By leveraging the intrinsic EIP properties of the DHN subsystems, the skew-symmetric nature of their interconnection structure, and LaSalle's invariance principle, we prove asymptotic stability of any feasible, hydraulic DHN equilibrium in a modular, bottom-up manner. This establishes a unifying framework for pressure and volume flow rate control, where multiple DHN subsystems, if EIP, can enter or leave the DHN in a *plug-and-play* fashion without having any impact on the stability properties of the hydraulic equilibrium. The main challenge behind this contribution was to deal with the nonlinear and differential-algebraic nature of the overall DHN closed-loop system.

The relevance of decentralized control designs for pressure and volume flow rate regulation is that they provide scalability and allow for an easy addition or removal of subsystems in a plug-and-play fashion without requiring communication, without adapting the other controllers in the DHN, and without endangering pressure and volume flow rate stability. Indeed, since stability is established modularly and independently of a communication protocol, decentralized controllers in general provide resilience against communication failure and preserve stability in case of unit malfunctions and topology changes.

In the literature, the field of decentralized, passivity-based hydraulic control of DHNs has recently been explored in [21]. However, the considered DHN model exhibits a number of restrictions, such as symmetric DHN topologies,[2] two temperature layers only, static pump models, no pressure holding units, and valves modeled as nonactuated components. Furthermore, pumps are assumed to be installed at every producer and every consumer, which excludes traditional DHNs in which consumers regulate their volume flow rates only via control valves. The same restrictions underlie the DHN models used in [14], [22], [23], and [24], where, additionally, only single producer DHNs are considered. Further noteworthy works that contribute toward a passivity-based control design and analysis of DHNs by introducing port-Hamiltonian system (PHS) models are [25] and [26]; see also [27], where water distribution networks are modeled as PHSs. However, Hauschild et al. [25] exhibit the same setup restrictions as [14], [22], [23], and [24], while Strehle et al. [26] overcome most of these restrictions with the exception of modeling valves as nonactuated components and considering pumps installed at every producer and consumer. Finally, pumps typically exhibit quadratic nonlinear behavior with model orders ranging between 1 and 5 [27], [28], [29]. To bridge the gap between the prevalent use of static pump models and the more complex nonlinear dynamics, we consider the linearized pump model in [26] and [28]. This allows the significant pump dynamics to be considered when analyzing the DHN stability. Note that Contribution 3 retains its validity when using more complex pump models as long as the same EIP properties are maintained.

[2]In symmetric DHN topologies, supply and return pipes are laid in parallel. This excludes practically relevant cases with meshed supply pipe networks and tree-like return pipe networks or more complex structures arising in multilayer topologies.

II. System Setup and Problem Description

In this section, we outline the general DHN setups that are covered by our approach and formally describe them as weakly connected digraphs. Subsequently, we describe the considered problem of decentralized pressure and volume flow rate regulation in DHNs.

A. DHN Setup and Digraph Representation

We describe DHNs as weakly connected digraphs $\mathcal{G} = (\mathcal{N}, \mathcal{E})$ without self-loops, as illustrated in Fig. 1. The edges $\mathcal{E}$ are partitioned into four sets: $\mathcal{D} = \{1, \ldots, D\}$, $D \geq 1$, represents the DGUs, $\mathcal{L} = \{D+1, \ldots, D+L\}$, $L \geq 1$, the consumers (loads), $\mathcal{P} = \{D+L+1, \ldots, D+L+P\}$, $P \geq 2$, the pipes, and $\mathcal{M} = \{D+L+P+1, \ldots, D+L+P+M\}$, $M \geq 0$, the mixing connections. Conventionally, the nodes $\mathcal{N}$ correspond to ideal system junctions interconnecting DGUs, consumers, and mixing connections with the pipe network of the DHN. At an ideal junction, all volume flow rates sum up to zero. However, in this work, we also view pressure holding units and elasticity capacitors arising from equipment in the DGU and consumer circuits as nodes. Therefore, we have $\mathcal{N} = \mathcal{H} \cup \mathcal{C} \cup \mathcal{K}$, where $\mathcal{H}$ are pressure holding units, $\mathcal{C}$ are elasticity capacitors, and $\mathcal{K}$ are the remaining ideal junctions. The orientation of the edges represents the arbitrary reference direction of positive flows. Moreover, for any $i \in \mathcal{E}$, $\mathcal{N}_i^-$ and $\mathcal{N}_i^+$ denote its source and target node, respectively. Analogously, for a given node $j \in \mathcal{N}$, $\mathcal{E}_j^-$ and $\mathcal{E}_j^+$ denote the sets of edges with j as source node and j as target node, respectively.

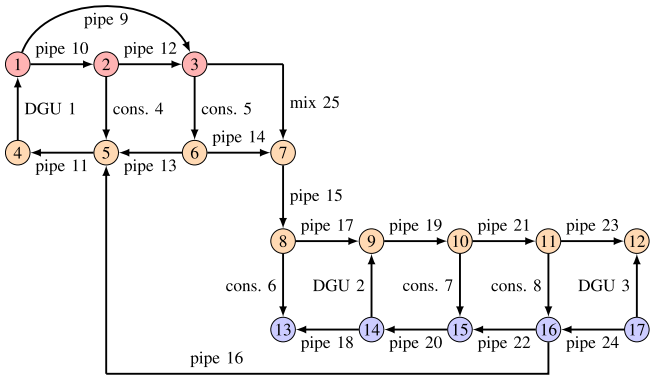

Fig. 1. Digraph representation of an exemplary DHN containing three DGUs $i \in \mathcal{D} = \{1, 2, 3\}$, five consumers $i \in \mathcal{L} = \{4, 5, 6, 7, 8\}$, 16 pipes $i \in \mathcal{P} = \{9, \ldots, 24\}$, and one mixing connection $i \in \mathcal{M} = \{25\}$ in a three-temperature layer topology indicated by the three different colors. The 17 nodes represent one pressure holding unit $j \in \mathcal{H} = \{4\}$, one ideal junction $j \in \mathcal{K} = \{7\}$, and 15 elasticity capacitors $j \in \mathcal{C} = \mathcal{N} \setminus \{4, 7\}$.

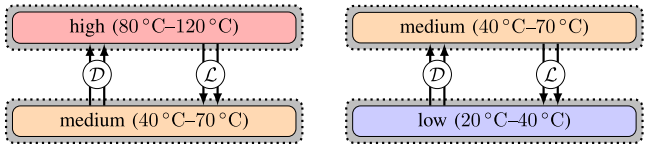

Fig. 2. Illustration of a traditional second- or third-generation DHN with high-temperature supply and medium-temperature return (left) and a fourth-generation DHN with medium-temperature supply and low-temperature return (right). Between the temperature layers may be an any number of $D \geq 1$ DGU and $L \geq 1$ consumer edges. The temperature layers coincide with the two hydraulic layers (gray dashed bubbles).

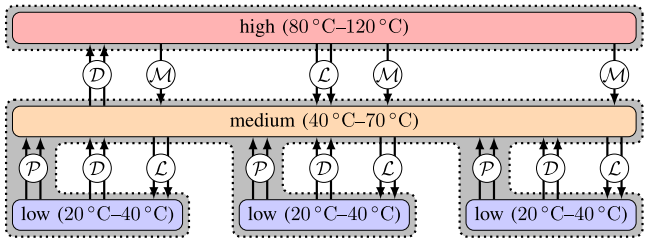

Fig. 3. Illustration of a DHN with the three temperature layers: high (red), medium (orange), low (blue), and the two hydraulic layers (gray dashed bubbles). Between the temperature layers may be any number of $D \geq 1$ DGU and $L \geq 1$ consumer edges. Between the high and medium layers may be any number of $M \geq 0$ mixing connections.

B. Temperature and Hydraulic Layers

As illustrated in Figs. 1–3, a DHN may comprise different temperature layers. We distinguish between three temperature layers, i.e., *high temperature* (80 °C–120 °C), *medium temperature* (40 °C–70 °C), and *low temperature* (20 °C–40 °C) [2], [4], [7, p. 44], [12], [13], [30, pp. 16–17]. The high- and medium-temperature layers form the supply and return of the dominating second- and third-generation DHNs, while the medium- and low-temperature layers form the supply and return of the emerging fourth-generation DHNs (see Fig. 2) [2], [30, pp. 16–17].

In future DHNs, the medium-temperature return of a second- or third-generation DHN may additionally serve as supply for (new) low-temperature DHN sections, yielding a three temperature layer topology, as illustrated in Figs. 1 and 3. Such low-temperature DHN sections allow to efficiently use the heat energy in a DHN (temperature cascading) and integrate renewable heat sources (e.g., waste heat, solar thermal, and heat pumps) and new consumers (e.g., low-energy buildings) into existing DHNs [7, p. 44], [11], [12], [13]. However, due to the ongoing trend of decreasing DHN temperatures, particularly during summer, the medium temperature might not be sufficiently high to cover the heat demand of some low-temperature consumers. Thus, low-temperature DHN sections in a three layer topology typically have at least one mixing connection, i.e., an edge $i \in \mathcal{M}$, that allows to boost the temperature by mixing high- with medium-temperature water (see node 7 in Fig. 1) [11], [12], [13].

Furthermore, in a three temperature layer topology, the low-temperature water is typically fed directly into the medium-temperature layer (see node 5 in Fig. 1 and the set of pipe edges $\mathcal{P}$ between low and medium temperature in Fig. 3) [11], [12], [13]. This implies that despite there possibly being three temperature layers, there are exactly two hydraulic layers (see Fig. 3). The number of hydraulic layers can be defined as follows.

Definition 1: A DHN has $n_l \geq 2$ hydraulic layers, where n_l is the number of weakly connected subgraphs $\mathcal{G}_1, \ldots, \mathcal{G}_{n_l}$ obtained by removing all edges $i \in \mathcal{D} \cup \mathcal{L} \cup \mathcal{M}$, i.e., all DGUs, consumers, and mixing connections, from $\mathcal{G}$.

C. Problem Description

In this article, we address the problem of pressure and flow rate regulation in DHNs via decentralized control schemes with plug-and-play capabilities. Specifically, the following hold.

1) For each DGU $i \in \mathcal{D}$, we aim at either regulating the differential pressure generated by pumps or regulating the volume flow rate using a combination of pump and valve. This is done to ensure that consumers have a sufficiently high pressure at their inlets and to adjust the heat injection into the DHN.
2) For each consumer $i \in \mathcal{L}$, the goal is to regulate the volume flow rate using valves or pumps. This is done to adjust the heat extraction by the consumers.
3) For each pipe $i \in \mathcal{P}_{\text{boost}} \subset \mathcal{P}$ with a pump in series, the objective is to counteract (frictional) differential pressure losses.
4) For each mixing connection $i \in \mathcal{M}$, the goal is to stabilize the volume flow rate through it to a desired set point and, thus, ensure a desired mixing ratio between high- and medium-temperature water streams.
5) For each pressure holding unit $j \in \mathcal{H}$, the goal is to regulate the pressure at the suction side of the circulation pump to prevent cavitation phenomena.

III. Hydraulic Modeling

With the DHN setup formalized as a digraph, we now present the models describing the hydraulic dynamics of the edges and nodes. First, we focus on the main actuators responsible for pressure and volume flow rate control, i.e., *pumps* and *valves*. They serve as building blocks for the hydraulic models of the DGU, *consumer*, *pipe*, and *mixing*

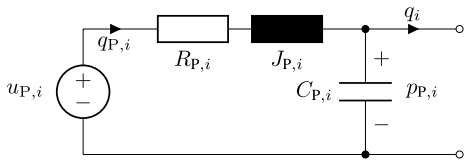

Fig. 4. Equivalent circuit of a linear, second-order approximation of pump dynamics (see [28]).

connection edges, as well as for the *pressure holding* nodes. The section concludes with the models of the *capacitive* and *simple junction* nodes. The latter models, being algebraic or *static* relations, cause the overall hydraulic DHN model to be of differential-algebraic form.

For the remainder of this article, we make the following modeling assumptions, which are valid under normal operating conditions (see also [14], [31]).

Assumption 1: The compressibility of water is neglected. Any reference and nominal pressure values as well as all model parameters are strictly positive. Pressure losses inside pipes $\lambda : \mathbb{R} \to \mathbb{R}$ and valves $\mu : \mathbb{R} \times \mathbb{R}_{\geq 0} \to \mathbb{R}$ caused by volume flow rates $q \in \mathbb{R}$ are continuously differentiable functions that are strictly monotonically increasing and satisfy $\lambda(q = 0) = 0$ and $\mu(q = 0, s) = 0$ for all valve stem positions $s \in \mathbb{R}_{\geq 0}$, respectively.

A. Hydraulic Actuators

1) Pumps: Pumps are the essential actuated components in DHNs. They are used for controlling the absolute pressure at specific points (pressure holding) (see [5], [7, pp. 54–55]), for (differential) pressure and volume flow rate control in DGUs (see [3], [5], [10], [14], [23]), for boosting the pressure in consumers and pipes (see [2], [14]), and for direct volume flow rate control in consumers (see [5], [9], [10]). In the prevalent literature (see the references above), pumps are considered as ideal pressure sources, which are analogous to voltage sources in dc networks. However, the dynamics of pumps, particularly the ones of centrifugal pumps that are widely used in DHNs [14], [24], lie in the range of several hundred milliseconds (see [28, Figs. 8 and 9]). Since this is a time scale comparable to that of the overall DHN hydraulics (see [4], [31]), a more accurate control design and system analysis must be performed if increasing numbers of pumps are integrated into DHNs.

As a starting point for such an improved design and analysis, we follow [26] and [28] and model each pump by a linear equivalent RLC circuit, as shown in Fig. 4. The RLC circuit arises by approximating the complex arrangement of power electronics, speed-controlled ac motor, and pump hydraulics by a linear second-order system. By applying Kirchhoff's voltage law (KVL) and Kirchhoff's current law (KCL) to Fig. 4, we obtain

$$\underbrace{\frac{\mathrm{d}}{\mathrm{d}t}\begin{bmatrix} J_{\mathrm{P},i} q_{\mathrm{P},i} \\ C_{\mathrm{P},i}\, p_{\mathrm{P},i} \end{bmatrix}}_{\dot{\boldsymbol{x}}_i} = \underbrace{\begin{bmatrix} -p_{\mathrm{P},i} - R_{\mathrm{P},i} q_{\mathrm{P},i} \\ q_{\mathrm{P},i} \end{bmatrix}}_{\boldsymbol{f}_i(\boldsymbol{x}_i)} + \underbrace{\begin{bmatrix} 1 \\ 0 \end{bmatrix}}_{\boldsymbol{G}_i(\boldsymbol{x}_i)} \underbrace{\begin{bmatrix} u_{\mathrm{P},i} \end{bmatrix}}_{u_i}$$
$$+ \underbrace{\begin{bmatrix} 0 \\ 1 \end{bmatrix}}_{\boldsymbol{K}_i} \underbrace{\begin{bmatrix} -q_i \end{bmatrix}}_{d_i} \tag{1a}$$

$$\boldsymbol{y}_i = \underbrace{\begin{bmatrix} q_{\mathrm{P},i} & p_{\mathrm{P},i} \end{bmatrix}^\top}_{\boldsymbol{h}_i(\boldsymbol{x}_i)}, \quad z_i = \underbrace{\begin{bmatrix} 0 & \frac{1}{C_{\mathrm{P},i}} \end{bmatrix}}_{\boldsymbol{T}_i} \boldsymbol{x}_i = p_{\mathrm{P},i} \tag{1b}$$

where $\boldsymbol{x}_i$ is the state vector, u_i the control input, and $\boldsymbol{y}_i$ the measurable output vector. The additional input d_i and output z_i model the interaction or physical interconnection between the pump and other subsystems, e.g., a DGU. Furthermore, $R_{\mathrm{P},i}$, $J_{\mathrm{P},i}$, and $C_{\mathrm{P},i}$ are the model parameters; $p_{\mathrm{P},i}$ is the pressure difference produced by the pump between its terminals; q_i is the volume flow rate through the pump; and $q_{\mathrm{P},i}$ is an auxiliary variable without physical interpretation. The control input $u_{\mathrm{P},i}$ can be interpreted as a pressure source originating from the rotational speed of the pump produced by an ac motor [28].[3]

2) Control Valves: Besides pumps, valves are the main actuators in DHNs. Their main task is the regulation of volume flow rates [3], [7, pp. 143–145 and 151], [30, pp. 19 and 29], [33]. In order to establish a desired volume flow rate q_i^*, valves adjust their pressure drop $\mu_i(s_{\mathrm{v},i}, q_i)$ by varying their stem position between fully closed ($s_{\mathrm{v},i} = 0$) and fully open ($s_{\mathrm{v},i} = 1$). Thus, they behave as variable, nonlinear flow resistors. In order to avoid volume surge behavior around their closing point, valves are designed, such that the stem has a lower limit just above zero in normal operation [7, p. 145]. Consequently, the following assumption can be made.

Assumption 2: In normal operation, the valve stem position is never zero, i.e., $s_{\mathrm{v},i} \in (0, 1]$.

The nonlinear characteristic pressure drop equation of any valve is given by [10, eq. (5)], [33, eq. (18)]

$$\mu_i(s_{\mathrm{v},i}, q_i) = \frac{1}{(C_{\mathrm{v},i} f_{\mathrm{v},i}(s_{\mathrm{v},i}))^2} |q_i| q_i \tag{2a}$$

where $s_{\mathrm{v},i} \in (0, 1]$ is the stem position, $q_i \in \mathbb{R}$ the volume flow rate through the valve, $C_{\mathrm{v},i} > 0$ the flow capacity of the valve, and $f_{\mathrm{v},i}(s_{\mathrm{v},i})$[4] the valve characteristic (see also the static orifice law [34, eq. (12)] or the definition of the so-called k_{v} value [7, p. 144]). By substituting

$$u_{\mathrm{v},i}\left(s_{\mathrm{v},i}\right) \coloneqq \frac{1}{f_{\mathrm{v},i}\left(s_{\mathrm{v},i}\right)^2}, \quad \hat{\mu}_i(q_i) \coloneqq \frac{1}{C_{\mathrm{v},i}^2} |q_i| q_i \tag{2b}$$

in (2a), the pressure drop can be written as follows:

$$\mu_i\left(s_{\mathrm{v},i}, q_i\right) = u_{\mathrm{v},i}\left(s_{\mathrm{v},i}\right) \hat{\mu}_i(q_i) \tag{3}$$

where $u_{\mathrm{v},i}(s_i) : (0, 1] \to \mathbb{R}_{>0}$ is a bijective mapping of the actual stem position $s_{\mathrm{v},i}$ to the virtual control input $u_{\mathrm{v},i}$,

[3]The choice of the variables $\boldsymbol{x}_i$, d_i, and z_i in (1) is based on the port-Hamiltonian [32, p. 114] representation of the system done in [26] (see [27] for a similar approach). We follow an analogous reasoning for the remaining DHN subsystems. In [1], we explicitly identify the port-Hamiltonian form of each of the DHN subsystems. Such a representation, which we skipped in this article due to space reasons, gives a clear perspective on which input–output ports are accessible for control and over which ports subsystems interact with each other. Furthermore, the passivity properties with respect to these ports and the Hamiltonian as storage function are directly visible.

[4]The two most common valve types are equal-percentage valves ($f_{\mathrm{v},i}(s_{\mathrm{v},i}) = R_i^{s_{\mathrm{v},i}-1}$ with rangeability $R_i > 0$) and linear valves ($f_{\mathrm{v},i}(s_{\mathrm{v},i}) = s_{\mathrm{v},i}$).

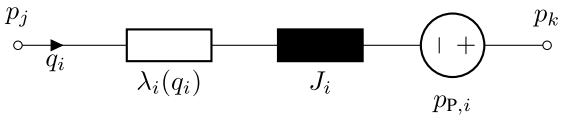

Fig. 5. Equivalent circuit of a hydraulic pipe model ($i \in \mathcal{P}$) with optional booster pump; $j \in \mathcal{N}_i^-$ and $k \in \mathcal{N}_i^+$.

and $\hat{\mu}_i(q_i)$ a continuously differentiable, strictly monotonically increasing function satisfying $\hat{\mu}_i(0) = 0$. Note that (3) is affine in the virtual control input $u_{\mathrm{v},i}$.

B. Edge Dynamics

1) Pipes: The hydraulic pipe model at an edge $i \in \mathcal{P}$ is illustrated in the equivalent circuit diagram in Fig. 5. Following the literature (see [8], [14], [23], [26], [35]), we model the pipe friction by a nonlinear, volume flow-dependent resistance $\lambda_i(q_i)$ (see Assumption 1) and the volume inertia by the linear inductance J_i. In contrast to prior works, we assume that some pipes might have booster pumps in series. Such pumps are represented by the voltage source in Fig. 5 and modeled by (1). By applying KVL and KCL to Fig. 5, we obtain the model for each $i \in \mathcal{P}$ as follows:

$$\underbrace{\frac{\mathrm{d}}{\mathrm{d}t}\begin{bmatrix} J_i q_i \\ J_{\mathrm{P},i} q_{\mathrm{P},i} \\ C_{\mathrm{P},i}\, p_{\mathrm{P},i} \end{bmatrix}}_{\boldsymbol{x}_i} = \underbrace{\begin{bmatrix} p_{\mathrm{P},i} - \lambda_i(q_i) \\ -p_{\mathrm{P},i} - R_{\mathrm{P},i} q_{\mathrm{P},i} \\ q_{\mathrm{P},i} - q_i \end{bmatrix}}_{\boldsymbol{f}_i(\boldsymbol{x}_i)} + \underbrace{\begin{bmatrix} 0 \\ 1 \\ 0 \end{bmatrix}}_{\boldsymbol{G}_i(\boldsymbol{x}_i)} \underbrace{\begin{bmatrix} u_{\mathrm{P},i} \end{bmatrix}}_{u_i} + \underbrace{\begin{bmatrix} 1 \\ 0 \\ 0 \end{bmatrix}}_{\boldsymbol{K}_i} \underbrace{\begin{bmatrix} p_j - p_k \end{bmatrix}}_{d_i} \tag{4a}$$

$$\boldsymbol{y}_i = \underbrace{\begin{bmatrix} q_i & q_{\mathrm{P},i} & p_{\mathrm{P},i} \end{bmatrix}^\top}_{\boldsymbol{h}_i(\boldsymbol{x}_i)}, \quad z_i = \underbrace{\begin{bmatrix} \frac{1}{J_i} & 0 & 0 \end{bmatrix}}_{\boldsymbol{T}_i} \boldsymbol{x}_i = q_i \tag{4b}$$

where $\boldsymbol{x}_i$ is the state vector, u_i the control input, $\boldsymbol{y}_i$ the measurable output vector, (d_i, z_i) the interaction (coupling) port pair, and $(j, k) \in \mathcal{N}_i^- \times \mathcal{N}_i^+$ are the source and target nodes of i with pressures p_j and p_k, respectively.

Remark 1: Any pipe $i \in \mathcal{P}$ without a booster pump can be modeled by (4) by fixing $u_{\mathrm{P},i} = p_{\mathrm{P},i} = 0$ and removing the part corresponding to the dynamics of $q_{\mathrm{P},i}$ and $p_{\mathrm{P},i}$.

2) DGUs: From a hydraulic viewpoint, a DGU may comprise two main parts, as illustrated in Fig. 6: a circulation circuit (red) [36], [37] and an optional pressure holding unit [7, pp. 54–55]. We view the circulation circuit in red as the actual edge $i \in \mathcal{D}$. It comprises a serial connection of a circulation pump, a control valve, pipes, and a heat exchanger. The circulation pump is modeled by (1). The control valve is modeled as a variable, nonlinear resistance $\hat{\mu}_i(q_i) u_{\mathrm{v},i}(s_{\mathrm{v},i})$ with control input $u_{\mathrm{v},i}(s_{\mathrm{v},i})$ as in (2). All pipes are lumped into the nonlinear, volume flow-dependent resistance $\lambda_i(q_i)$ and the inductance J_i, which represent the pipe friction and volume inertia, respectively. By applying KVL and KCL to the red part in Fig. 6, we obtain the model for each $i \in \mathcal{D}$

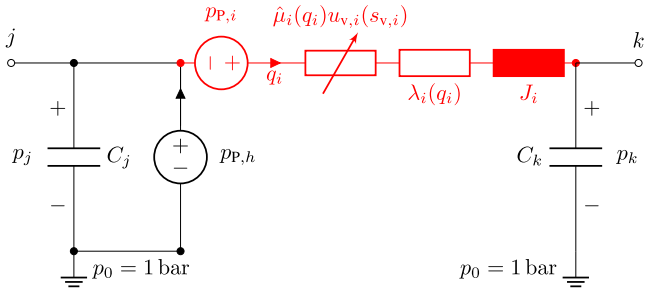

Fig. 6. Equivalent circuit of a hydraulic DGU model ($i \in \mathcal{D}$) with pressure holding (black voltage source) and circulation circuit (red) [26, Fig. 2]; without loss of generality, the capacitance C_j may be lumped with the pressure holding (see Section III-C1); $j \in \mathcal{N}_i^-$ and $k \in \mathcal{N}_i^+$.

as follows:

$$\underbrace{\frac{\mathrm{d}}{\mathrm{d}t}\begin{bmatrix} J_i q_i \\ J_{\mathrm{P},i} q_{\mathrm{P},i} \\ C_{\mathrm{P},i}\, p_{\mathrm{P},i} \end{bmatrix}}_{\boldsymbol{x}_i} = \underbrace{\begin{bmatrix} p_{\mathrm{P},i} - \lambda_i(q_i) \\ -p_{\mathrm{P},i} - R_{\mathrm{P},i} q_{\mathrm{P},i} \\ q_{\mathrm{P},i} - q_i \end{bmatrix}}_{\boldsymbol{f}_i(\boldsymbol{x}_i)} + \underbrace{\begin{bmatrix} -\hat{\mu}_i(q_i) & 0 \\ 0 & 1 \\ 0 & 0 \end{bmatrix}}_{\boldsymbol{G}_i(\boldsymbol{x}_i)} \underbrace{\begin{bmatrix} u_{\mathrm{v},i} \\ u_{\mathrm{P},i} \end{bmatrix}}_{\boldsymbol{u}_i} + \underbrace{\begin{bmatrix} 1 \\ 0 \\ 0 \end{bmatrix}}_{\boldsymbol{K}_i} \underbrace{\begin{bmatrix} p_j - p_k \end{bmatrix}}_{d_i} \tag{5a}$$

$$\boldsymbol{y}_i = \underbrace{\begin{bmatrix} q_i & q_{\mathrm{P},i} & p_{\mathrm{P},i} \end{bmatrix}^\top}_{\boldsymbol{h}_i(\boldsymbol{x}_i)}, \quad z_i = \underbrace{\begin{bmatrix} \frac{1}{J_i} & 0 & 0 \end{bmatrix}}_{\boldsymbol{T}_i} \boldsymbol{x}_i = q_i \tag{5b}$$

where $\boldsymbol{x}_i$ is the state vector, $\boldsymbol{u}_i$ the control input vector, $\boldsymbol{y}_i$ the measurable output vector, (d_i, z_i) the interaction (coupling) port pair, and $(j, k) \in \mathcal{N}_i^- \times \mathcal{N}_i^+$ are the source and target nodes of i with pressures p_j and p_k, respectively.

Remark 2: The pressure holding unit of a given DGU is represented by the (black) voltage source $p_{\mathrm{P},h}$ shown in Fig. 6. The capacitances C_j and C_k model the hydraulic elasticity of all the components in the DGU circulation circuit, particularly of the heat exchanger (see [34], [38]). For simplicity, we assume that C_j is lumped with $C_{\mathrm{P},h}$ of the pressure holding (see Fig. 4). Furthermore, to clearly describe the network interconnection among all the subsystems in the DHN, we view the pressure holding and the elasticity capacitances as nodes of the DHN graph; we elaborate on their models in Section III-C.

3) Consumers: Nowadays, most of the consumers are connected indirectly to a DHN via heat exchangers in series with pipes and a control valve for volume flow rate control [7, pp. 87 and 143]. In future DHNs, however, additional pumps are expected to be included in some (up to all) consumer circuits: either for pressure boosting to ensure a proper functioning of the control valves under unclear and changing hydraulic conditions [2], [14] or in DHNs operated with DVSPs [5], [9], [10]. Consequently, the hydraulic consumer circuit at an edge $i \in \mathcal{L}$ is modeled similar to the hydraulic DGU circulation circuit (red part in Fig. 7, and see [8, Fig. 2]). The only differences are on the working direction of the pump and the sign convention of the volume flow rate, which is reflected in the edge orientation in the DHN digraph (see Fig. 1 and [7, pp. 87 and 143]). Furthermore, pressure holding units

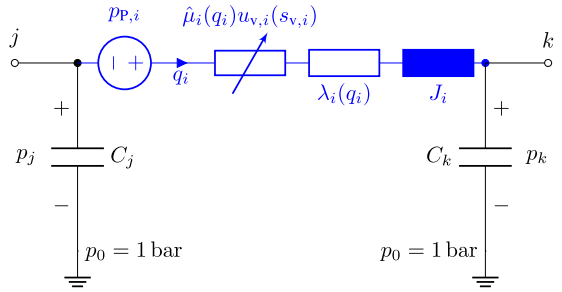

Fig. 7. Equivalent circuit of a hydraulic consumer model ($i \in \mathcal{L}$) [8, Fig. 2]; $j \in \mathcal{N}_i^-$ and $k \in \mathcal{N}_i^+$.

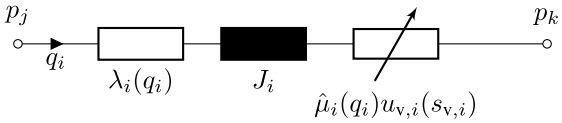

Fig. 8. Equivalent circuit of a hydraulic mixing connection model ($i \in \mathcal{M}$); $j \in \mathcal{N}_i^-$ and $k \in \mathcal{N}_i^+$.

are typically not installed at consumers. By applying KVL and KCL to Fig. 7, we obtain the model for each consumer $i \in \mathcal{L}$ as in (5).

Remark 3: Any consumer $i \in \mathcal{L}$ without a pump can be modeled by (5) by fixing $u_{\mathrm{P},i} = p_{\mathrm{P},i} = 0$ and removing the part corresponding to the dynamics of $q_{\mathrm{P},i}$ and $p_{\mathrm{P},i}$. Such consumers regulate their flow rate through their respective control valve.

4) Mixing Connection: As outlined in Section II-B, future DHNs may have a topology with three temperature layers. In order to guarantee a sufficient heat supply to the low-temperature sections, the medium-temperature water is typically mixed with high-temperature water via a mixing connection before it is fed into the low-temperature section (see node 7 in Fig. 1). The hydraulic circuit of a mixing connection at an edge $i \in \mathcal{M}$ is illustrated in Fig. 8. It comprises a pipe in series with a control valve. By applying KVL to Fig. 8, we obtain the model for each $i \in \mathcal{M}$ as follows:

$$\frac{\mathrm{d}}{\mathrm{d}t}\underbrace{\left[J_i q_i\right]}_{x_i} = \underbrace{\left[-\lambda_i(q_i)\right]}_{f_i(x_i)} + \underbrace{\left[-\hat{\mu}_i(q_i)\right]}_{G_i(\boldsymbol{x}_i)}\underbrace{\left[u_{\mathrm{v},i}\right]}_{u_i} + \underbrace{\left[1\right]}_{K_i}\underbrace{\left[p_j - p_k\right]}_{d_i} \tag{6a}$$

$$y_i = \underbrace{q_i}_{h_i(x_i)}, \quad z_i = \underbrace{\left[\tfrac{1}{J_i}\right]}_{T_i} x_i = q_i \tag{6b}$$

where x_i is the state, u_i the control input, y_i the measurable output, (d_i, z_i) the interaction (coupling) port pair, and $(j,k) \in \mathcal{N}_i^- \times \mathcal{N}_i^+$ are the source and target nodes of i with pressures p_j and p_k, respectively.

C. Node Models

As outlined in Sections II-A, III-B2, and III-B3, the set of nodes $\mathcal{N}$ of the DHN graph $\mathcal{G} = (\mathcal{N}, \mathcal{E})$ is the union of three disjoint sets

$$\mathcal{N} = \mathcal{H} \cup \mathcal{C} \cup \mathcal{K} \tag{7}$$

where $\mathcal{H}$ is the set of pressure holding units, $\mathcal{C}$ is the set of elasticity capacitances, and $\mathcal{K}$ is the set of simple junctions.

1) Pressure Holding: Pressure holding units are realized technically in two ways: dynamic pressure holding with a pressure dictation pump and static pressure holding with a closed vessel [7, pp. 54–56]. Furthermore, pressure holding units are almost exclusively installed on the suction side of circulation pumps (prepressure control) (see Fig. 6) and are instrumental in preventing cavitation [7, pp. 54–55], [17].

Dynamic pressure holding is typically conducted in larger DGUs with powerful circulation pumps. It is realized by a pressure dictation pump located between a pressurized container and the DHN [7, pp. 54–55], [39, Fig. 1]. As outlined in Section III-A1, we approximate the dynamics of any pump by the linear second-order system (1). Thus, the case in which a dynamic pressure holding unit is installed at a DGU $i \in \mathcal{D}$ is equivalent to replacing the black voltage source in Fig. 6 by the RLC circuit in Fig. 4. Note that in contrast to the circulation pump, which is coupled with the circulation circuit (red part in Fig. 6), the black voltage source already represents the entire pressure holding unit, i.e., we assume that the dictation pump is lumped together with the pressurized container. Thus, the model for each $j \in \mathcal{H}$ is similar to (1) and given by

$$\begin{aligned}\frac{\mathrm{d}}{\mathrm{d}t}\underbrace{\begin{bmatrix} J_{\mathrm{P},j} q_{\mathrm{P},j} \\ C_{\mathrm{P},j} p_{\mathrm{P},j} \end{bmatrix}}_{\boldsymbol{x}_j} &= \underbrace{\begin{bmatrix} -p_{\mathrm{P},j} - R_{\mathrm{P},j} q_{\mathrm{P},j} \\ q_{\mathrm{P},j} \end{bmatrix}}_{\boldsymbol{f}_j(\boldsymbol{x}_j)} + \underbrace{\begin{bmatrix} 1 \\ 0 \end{bmatrix}}_{\boldsymbol{G}_j(\boldsymbol{x}_j)}\underbrace{\begin{bmatrix} u_{\mathrm{P},j} \end{bmatrix}}_{u_j} \\ &\quad + \underbrace{\begin{bmatrix} 0 \\ 1 \end{bmatrix}}_{\boldsymbol{K}_j}\underbrace{\sum_{i \in \mathcal{I}_j} q_i}_{d_j}\end{aligned} \tag{8a}$$

$$\boldsymbol{y}_j = \underbrace{\begin{bmatrix} q_{\mathrm{P},j} & p_{\mathrm{P},j} \end{bmatrix}^\top}_{\boldsymbol{h}_j(\boldsymbol{x}_j)}, \quad z_j = \underbrace{\begin{bmatrix} 0 & \frac{1}{C_{\mathrm{P},j}} \end{bmatrix}}_{\boldsymbol{T}_j}\boldsymbol{x}_j = p_{\mathrm{P},j} \tag{8b}$$

where $\boldsymbol{x}_j$ is the state vector, u_j the control input, $\boldsymbol{y}_j$ the measurable output vector, (d_j, z_j) the interaction (coupling) port pair, and $\mathcal{I}_j \subseteq \mathcal{E}$ the set of edges that are incident to j.

Remark 4: A static pressure holding is used in smaller DGUs with compact circulation pumps. It is realized by directly adding a closed, pressurized vessel. In an equivalent circuit perspective, this can be understood as a preloaded capacitor. Thus, in case of static pressure holding, we simply replace the black voltage source in Fig. 6 with a capacitor $C_{\mathrm{P},h}$ that we consider to be lumped with C_j.

2) Capacitive Nodes: Invoking the volume balance, we obtain the model for each $j \in \mathcal{C}$ as follows:

$$\frac{\mathrm{d}}{\mathrm{d}t}\underbrace{\left[C_j p_j\right]}_{x_j} = \underbrace{\left[1\right]}_{K_j}\underbrace{\sum_{i \in \mathcal{I}_j} q_i}_{d_j} \tag{9a}$$

$$z_j = \underbrace{\left[\tfrac{1}{C_j}\right]}_{T_j} x_j = p_j \tag{9b}$$

where x_j is the state, (d_j, z_j) the interaction (coupling) port pair, and $\mathcal{I}_j$ the set of edges that are incident to j.

3) Simple Junctions: The model for each $j \in \mathcal{K}$ is analogous to (9) with C_j fixed to zero and treating $z_j = p_j$ as an algebraic variable. Note that there is no state variable to describe the behavior of simple junctions.

IV. Problem Formulation and Approach

Having modularly defined the overall DHN model, we proceed to formally stating the main pressure and volume flow rate control problems addressed in this work. Afterward, we give an overview of the EIP-based approach taken to solve these problems via decentralized control design. In the sequel, $\bar{(\cdot)}$ denotes any variable in steady state, whereas $(\cdot)^*$ denotes a desired set point that is to be established in steady state.

For the case of DGUs, we adopt the terminology of electrical power systems and suppose that they may operate either in *grid-forming* or *grid-feeding* mode $i \in \mathcal{D} = \mathcal{D}_{\text{form}} \cup \mathcal{D}_{\text{feed}}$. DGUs in grid-forming mode $i \in \mathcal{D}_{\text{form}}$ actively form the hydraulic conditions required to operate DHNs by regulating the differential pressure generated by their circulation pumps to desired set points $p^*_{\text{P},i}$ [7, pp. 47–48], [40]. In this case, the control valves in their circulation circuits are fully open, i.e., $\bar{u}_{\text{v},i} = u_{\text{v},i}(s_{\text{v},i} = 1)$. DGUs in grid-feeding mode $i \in \mathcal{D}_{\text{valve}} \subseteq \mathcal{D}_{\text{feed}}$ regulate the volume flow rate through their circulation circuits to desired set points q_i^* by means of their control valves. Under approximately constant water temperature, this is equivalent to controlling the thermal energy they feed into the DHN (see [36], [41], [42, Sec. 2.3]). Note that for a proper functioning of the control valve, the circulation pump still introduces some differential pressure $p^*_{\text{P},i}$, which is then throttled by the control valve, such that the desired volume flow rate q_i^* is reached. To guarantee feasible operating modes of the DHN subsystems, the following assumption is introduced (see [1, Proposition 1] for more details).

Assumption 3: $\mathcal{D}_{\text{form}} \neq \emptyset$.

Consumers $i \in \mathcal{L}$ regulate the thermal energy they consume by controlling their volume flow rates to desired set points q_i^* [7, pp. 143–145 and 151], [30, p. 29]. Traditionally, this is done by control valves only. The set of consumers for which $u_{\text{v},i}(s_{\text{v},i})$ is the main control input is, thus, denoted by $\mathcal{L}_{\text{valve}} \subseteq \mathcal{L}$. However, as discussed in Section III-B3, booster pumps might be added to some consumer circuits. We identify these consumers by the set $\mathcal{L}_{\text{boost}} \subseteq \mathcal{L}$. In each consumer $i \in \mathcal{L}_{\text{boost}}$, the pump pressure is controlled to some desired set point $p^*_{\text{P},i}$, which is then throttled by the control valve, such that the desired volume flow rate q_i^* is reached.

Remark 5: In some DHNs with DVSPs, it is suggested to directly conduct the volume flow rate control in DGUs $i \in \mathcal{D}_{\text{VSP}} \subseteq \mathcal{D}_{\text{feed}}$ and consumers $i \in \mathcal{L}_{\text{VSP}} \subseteq \mathcal{L}$ by pumps without including control valves in the respective hydraulic circuits [5], [9].[5] In [10], a hybrid DVSP setup is proposed in which all DGUs and some consumers have only pumps, while some consumers have only control valves. Consequently, it is apparent that depending on the topology and producer–consumer configuration, different hydraulic designs of DGU and consumer circuits might be beneficial. Thus, in this work, we consider all possible combinations of designs (see Problem 1).

For *pipes* $i \in \mathcal{P}$, we denote by $\mathcal{P}_{\text{boost}} \subseteq \mathcal{P}$ the subset of pipes that have a *booster pump* connected in series. These pumps are in charge of counteracting the differential pressure loss over the corresponding pipe by introducing a differential pressure $p^*_{\text{P},i}$. *Mixing connections* $i \in \mathcal{M}$ control their volume flow rates to desired set points q_i^* to establish a desired mixing ratio of high- and medium-temperature water (see Section III-B4). Pressure holding units $j \in \mathcal{H}$ regulate the pressure p_j at the suction side of the circulation pump of their associated DGUs $j \in \mathcal{N}_i^-$ (see Fig. 6) to a suitable set point $p_j^* = p^*_{\text{P},h}$. This pressure also serves as the static pressure in a DHN (see [7, p. 55]).

In summary, we note that the control tasks amount to pressure and volume flow rate control of pumps and volume flow rate control of valves.

Problem 1: Consider a DHN as described in Section III. Design decentralized controllers for the pumps and valves in the actuated subsystems $i \in \mathcal{D} \cup \mathcal{L} \cup \mathcal{P}_{\text{boost}} \cup \mathcal{M} \cup \in \mathcal{H}$, such that hydraulic equilibria with the following characteristics are asymptotically stabilized.

1) For each DGU $i \in \mathcal{D}_{\text{form}}$ [see (5)], $u_{\text{v},i}(s_{\text{v},i} = 1) = 1 = \bar{u}_{\text{v},i}$ is fixed, and $u_{\text{P},i}$ is such that $\bar{p}_{\text{P},i} = p^*_{\text{P},i} > 0$.
2) For each DGU $i \in \mathcal{D}_{\text{valve}}$ [see (5)], $u_{\text{P},i}$ and $u_{\text{v},i}$ are such that $\bar{p}_{\text{P},i} = p^*_{\text{P},i} > 0$ and $\bar{q}_i = q_i^* > 0$.
3) For each DGU $i \in \mathcal{D}_{\text{VSP}}$ [see (5)], $u_{\text{v},i}(s_{\text{v},i} = 1) = 1 = \bar{u}_{\text{v},i}$ is fixed, and $u_{\text{P},i}$ is such that $\bar{q}_i = q_i^* > 0$.
4) For each consumer $i \in \mathcal{L}_{\text{boost}}$ [see (5)], $u_{\text{P},i}$ and $u_{\text{v},i}$ are such that $\bar{p}_{\text{P},i} = p^*_{\text{P},i} > 0$ and $\bar{q}_i = q_i^* > 0$.
5) For each consumer $i \in \mathcal{L}_{\text{valve}}$ [see (5)], $u_{\text{P},i} = 0$ is fixed, and $u_{\text{v},i}$ is such that $\bar{q}_i = q_i^* > 0$.
6) For each consumer $i \in \mathcal{L}_{\text{VSP}}$ [see (5)], $u_{\text{v},i}(s_{\text{v},i} = 1) = 1 = \bar{u}_{\text{v},i}$ is fixed, and $u_{\text{P},i}$ is such that $\bar{q}_i = q_i^* > 0$.
7) For each pipe $i \in \mathcal{P}_{\text{boost}}$ [see (4)], $u_{\text{P},i}$ is such that $\bar{p}_{\text{P},i} = p^*_{\text{P},i} > 0$.
8) For each mixing connection $i \in \mathcal{M}$ [see (6)], $u_{\text{v},i}$ is such that $\bar{q}_i = q_i^* > 0$.
9) For each pressure holding unit $j \in \mathcal{H}$ [see (8)], $u_{\text{P},j}$ is such that $\bar{p}_{\text{P},j} = p^*_{\text{P},j} > 0$.

Remark 6: Note that similar to the hierarchical control of power systems, the set points of the volume flow rates and pressures are assumed to be known and specified by a higher level control. However, showing the existence of equilibrium points for given desired set points is not a trivial task in view of the nonlinear nature of the equilibrium equations and is not the focus of this manuscript. The interested reader is referred to for example [43], where hydraulic equilibria are computed using global and local system information.

A. Approach

In order to address Problem 1, we recall from Section III that the dynamics of any edge or node subsystem $i \in \mathcal{E} \cup \mathcal{N}$ of a DHN, with the exception of simple junctions, can be written in the general form

$$\dot{\boldsymbol{x}}_i = \boldsymbol{f}_i(\boldsymbol{x}_i) + \boldsymbol{G}_i(\boldsymbol{x}_i)\boldsymbol{u}_i + \boldsymbol{K}_i d_i$$
$$\boldsymbol{y}_i = \boldsymbol{h}_i(\boldsymbol{x}_i), \quad z_i = \boldsymbol{T}_i \boldsymbol{x}_i.$$

[5]To avoid cluttering notation, we assume that valves in DGUs and consumers with DVSPs are still there, however fully open, i.e., $\bar{u}_{\text{v},i} = u_{\text{v},i}(s_{\text{v},i} = 1)$.

Then, inspired by Strehle et al. [8], [45] and Arcak et al. [44, Th. 3.1], we take a modular, bottom-up approach and design decentralized passivity-based controllers for the actuated subsystems specified in Problem 1. These controllers take the form

$$\dot{\boldsymbol{\xi}}_i = \boldsymbol{\pi}_i(\boldsymbol{y}_i, \boldsymbol{\xi}_i), \;\; \boldsymbol{u}_i = \boldsymbol{c}_i(\boldsymbol{y}_i, \boldsymbol{\xi}_i)$$

and act on the pumps and valves, such that each closed-loop subsystem $i \in \mathcal{D} \cup \mathcal{L} \cup \mathcal{P}_{\text{boost}} \cup \mathcal{M} \cup \mathcal{H}$ fulfills its respective steady-state characteristic from 1)–5) in Problem 1.

Moreover, each controller is such that the associated closed-loop subsystem is EIP with respect to its interaction port pair (d_i, z_i) and some positive definite storage function. That is, it is to be shown that for any feasible equilibrium pair $(\bar{\hat{\boldsymbol{x}}}_i, \bar{d}_i)$ with $\hat{\boldsymbol{x}}_i = [\boldsymbol{x}_i^\top, \boldsymbol{\xi}_i^\top]^\top$ the augmented closed-loop state vector fulfilling the respective requirement 1)–5) in Problem 1, there exists a scalar function $\hat{\boldsymbol{x}}_i \mapsto \hat{H}_i(\hat{\boldsymbol{x}}_i)$ that is positive definite with respect to any feasible equilibrium $\bar{\hat{\boldsymbol{x}}}_i$ and satisfies $\dot{\hat{H}}_i(\hat{\boldsymbol{x}}_i) \leq (d_i - \bar{d}_i)(z_i - \bar{z}_i)$. A subsequent step consists of showing that the interconnection among the DHN subsystems is power-preserving, i.e., it satisfies $\sum_{i \in \mathcal{E} \cup \mathcal{N}} (d_i - \bar{d}_i)(z_i - \bar{z}_i) = 0$, which makes $\sum_{i \in \mathcal{E} \cup \mathcal{N}} \hat{H}_i(\hat{\boldsymbol{x}}_i, \hat{\boldsymbol{x}}_i)$ a Lyapunov function for any feasible, hydraulic, closed-loop DHN equilibrium and, thus, ensures its stability. *Asymptotic stability* is then investigated either by invoking LaSalle's invariance principle or checking for strict EIP of all subsystems.

V. Passivity-Based Control Design

In the first part of this section, we develop decentralized, passivity-based controllers for pumps and valves. In the second part, we deploy the controlled pumps and valves to each of the actuated DHN subsystems (DGUs, consumers, booster pumps, and so on) and show that the resulting closed-loop dynamics are EIP with respect to the interaction ports. As stated in Section VI-A, this paves the way for our bottom-up, modular stability analysis that we present in the sequel.

A. Pressure and Volume Flow Rate Control of Pumps

Instrumental to solving Problem 1 is the ability to regulate the pressure $p_{\text{P},i}$ or the volume flow rate q_i of a given pump in the subsystems $i \in \mathcal{D} \cup \mathcal{L}_{\text{boost}} \cup \mathcal{L}_{\text{VSP}} \cup \mathcal{P}_{\text{boost}} \cup \mathcal{H}$ toward desired constant set points. For the control design, we initially consider the isolated pump model (1) and address pressure and volume flow rate regulation. Then, the closed-loop pump dynamics are interconnected to the respective subsystems $\mathcal{D} \cup \mathcal{L}_{\text{boost}} \cup \mathcal{L}_{\text{VSP}} \cup \mathcal{P}_{\text{boost}} \cup \mathcal{H}$.

1) Pressure Control of Pumps: For the pump pressure $p_{\text{P},i}$, we propose a controller for $u_{\text{P},i}$ that is based on algebraic IDA [18] passivity-based control extended with integral action on the nonpassive output of the pump model [19].

Proposition 1: Consider the pump model (1). Assign the control input $u_{\text{P},i}$ as follows:

$$Q_{\text{I},i}\dot{r}_i = \left(p_{\text{P},i} - p_{\text{P},i}^*\right) \tag{10a}$$

$$\chi_i = q_{\text{P},i} + r_i \tag{10b}$$

$$\nu_i = -p_{\text{P},i} - R_{\text{P},i} q_{\text{p},i} + \tfrac{J_{\text{P},i}}{Q_{\text{I},i}}\left(p_{\text{P},i} - p_{\text{P},i}^*\right) \tag{10c}$$

$$u_{\text{P,i}} = -\nu_i - R_i^{\text{p}} \chi_i - p_{\text{P},i} \tag{10d}$$

where r_i is a controller state, $p_{\text{P},i}^* > 0$ is a pressure set point, and R_i^{p}, $Q_{\text{I},i} > 0$ are control parameters. Then, the closed-loop system is given by

$$\frac{\text{d}}{\text{d}t}\underbrace{\begin{bmatrix} J_{\text{P},i}\chi_i \\ C_{\text{P},i}p_{\text{P},i} \\ Q_{\text{I},i}r_i \end{bmatrix}}_{\boldsymbol{x}_i^{\text{p}}} = \underbrace{\begin{bmatrix} -R_i^{\text{p}}\chi_i - \left(p_{\text{P},i} - p_{\text{P},i}^*\right) \\ \chi_i - r_i \\ p_{\text{P},i} - p_{\text{P},i}^* \end{bmatrix}}_{f_i^{\text{p}}(\boldsymbol{x}_i^{\text{p}})} + \underbrace{\begin{bmatrix} 0 \\ 1 \\ 0 \end{bmatrix}}_{\boldsymbol{\kappa}_i^{\text{p}}} d_i \tag{11a}$$

$$z_i = p_{\text{P},i}. \tag{11b}$$

Moreover, (11) is EIP with supply rate $(z_i - \bar{z}_i)(d_i - \bar{d}_i)$ and positive definite storage function

$$H_i^{\text{p}} = \tfrac{1}{2}\|\boldsymbol{x}_i^{\text{p}} - \bar{\boldsymbol{x}}_i^{\text{p}}\|^2_{\text{diag}^{-1}(J_{\text{P},i}, C_{\text{P},i}, Q_{\text{I},i})} \tag{12}$$

for any (feasible) equilibrium pair $(\bar{d}_i, \bar{z}_i)$ and associated equilibrium state

$$\bar{\boldsymbol{x}}_i^{\text{p}} = \left[J_{\text{P},i}\bar{\chi}_i \;\; C_{\text{P},i}p_{\text{P},i}^* \;\; Q_{\text{I},i}\bar{r}_i\right]^\top. \tag{13}$$

Proof: See Appendix A. ∎

Remark 7: The controller (10) is decentralized, as it only requires knowledge of local variables and parameters, such as $q_{\text{P},i}$, $p_{\text{P},i}$, and $J_{\text{P},i}$. Observe, in particular, that if we choose $R_i^{\text{p}} = R_{\text{P},i}$, (10) becomes independent of $q_{\text{P},i}$. This is desired as $q_{\text{P},i}$ does not represent a physical quantity. Moreover, note that (10d) can be written as follows:

$$\begin{aligned} u_{\text{P},i} = {} & \left(-R_i^{\text{p}} + R_{\text{P},i}\right)q_{\text{P},i} + R_i^{\text{p}} Q_{\text{I},i}^{-1}\int_0^t \left(p_{\text{P},i}^* - p_{\text{P},i}\right)\text{d}t \\ & + J_{\text{P},i}Q_{\text{I},i}^{-1}\left(p_{\text{P},i}^* - p_{\text{P},i}\right) \end{aligned} \tag{14}$$

which clearly illustrates its composition as the combination of a state feedback term and a PI term.

2) Volume Flow Rate Control via Pumps: Next, we address the task of achieving volume flow rate control of pipes or heat exchangers via pumps. For this, we focus on the model of a pump in series with a pipe element, which is equivalent to (4) but with d_i treated as an arbitrary external input.

Proposition 2: Consider the model of any pump in series with a pipe element [see (4)]. Assign $u_{\text{P},i}$ as follows:

$$Q_{\text{I},i}\dot{r}_i = \left(q_i - q_i^*\right) \tag{15a}$$

$$u_{\text{P},i} = -K_{\text{P},i}p_{\text{P},i} - r_i \tag{15b}$$

where r_i is a controller state, $q_i^* > 0$ is a volume flow rate set point, and $Q_{\text{I},i}$, $K_{\text{P},i}$ are control parameters satisfying

$$Q_{\text{I},i} > 0, \quad 0 < Q_{\text{I},i}\left(K_{\text{P},i} + 1\right) - C_{\text{P},i} =: \kappa_i^{\text{f}}. \tag{16}$$

Then, the closed-loop system is given by

$$\frac{\text{d}}{\text{d}t}\underbrace{\begin{bmatrix} J_i q_i \\ J_{\text{P},i}q_{\text{P},i} \\ C_{\text{P},i}p_{\text{P},i} \\ Q_{\text{I},i}r_i \end{bmatrix}}_{\boldsymbol{x}_i^{\text{f}}} = \underbrace{\begin{bmatrix} p_{\text{P},i} - \lambda_i(q_i) \\ -p_{\text{P},i} - R_{\text{P},i}q_{\text{P},i} - K_{\text{P},i}p_{\text{P},i} - r_i \\ q_{\text{P},i} - q_i \\ q_i - q_i^* \end{bmatrix}}_{f_i^{\text{f}}(\boldsymbol{x}_i^{\text{f}})}$$

$$+ \underbrace{\begin{bmatrix} 1 \\ 0 \\ 0 \\ 0 \end{bmatrix}}_{K_i^{\mathrm{f}}} d_i \tag{17a}$$

$$z_i = q_i. \tag{17b}$$

Moreover, (17) is EIP with supply rate $(z_i - \bar{z}_i)(d_i - \bar{d}_i)$ and positive definite storage function

$$H_i^{\mathrm{f}} = \tfrac{1}{2}\|x_i^{\mathrm{f}} - \bar{x}_i^{\mathrm{f}}\|^2_{Q_i^{\mathrm{f}}} \tag{18a}$$

$$Q_i^{\mathrm{f}} = \begin{bmatrix} \frac{1}{J_i} & 0 & 0 & 0 \\ 0 & \frac{Q_{\mathrm{I},i}}{J_{\mathrm{P},i}\kappa_i^{\mathrm{f}}} & 0 & 0 \\ 0 & 0 & \frac{1}{C_{\mathrm{P},i}} + \frac{1}{\kappa_i^{\mathrm{f}}} & \frac{1}{\kappa_i^{\mathrm{f}}} \\ 0 & 0 & \frac{1}{\kappa_i^{\mathrm{f}}} & \frac{1}{\kappa_i^{\mathrm{f}}} \end{bmatrix} \tag{18b}$$

for any (feasible) equilibrium pair $(\bar{d}_i, \bar{z}_i)$ and associated equilibrium state

$$\bar{x}_i^{\mathrm{f}} = \begin{bmatrix} J_i q_i^* & J_{\mathrm{P},i} q_i^* & C_{\mathrm{P},i}\bar{p}_{\mathrm{P},i} & Q_{\mathrm{I},i}\bar{r}_i \end{bmatrix}^\top. \tag{19}$$

Proof: See Appendix B. ∎

Remark 8: The controller (15), which is inspired by Nahata et al. [46, Th. 2], is used in the sequel for flow control in some DGUs and some consumers. Note that the dynamics (5) of DGUs and consumers are equivalent to the dynamics (4) of a pipe element in series with a pump, excluding the control valve.

B. Volume Flow Rate Control of Valves

Problem 1 also considers the regulation of volume flow rates q_i through DGUs, consumers, and mixing connections via control valves. Note that the model of a control valve in series with a pipe element is equivalent to (6), but with d_i treated as an arbitrary external input.

Proposition 3: Consider the model of any control valve in series with a pipe element [see (6)]. Let

$$\hat{y}_{\mathrm{v},i} = -\hat{\mu}_i(q_i)\big(q_i - q_i^*\big) \tag{20}$$

and assign the control input $u_{\mathrm{v},i}$ as follows:

$$Q_{\mathrm{I},i}\dot{r}_i = -\hat{y}_{\mathrm{v},i} \tag{21a}$$

$$u_{\mathrm{v},i} = -K_{\mathrm{P},i}\hat{y}_{\mathrm{v},i} + r_i \tag{21b}$$

where r_i is a controller state, $q_i^* > 0$ is a volume flow rate set point, and $Q_{\mathrm{I},i}$, $K_{\mathrm{P},i} > 0$ are control parameters. Then, the closed-loop system is given by

$$\frac{\mathrm{d}}{\mathrm{d}t}\underbrace{\begin{bmatrix} J_i q_i \\ Q_{\mathrm{I},i} r_i \end{bmatrix}}_{x_i^{\mathrm{v}}} = \underbrace{\begin{bmatrix} -\lambda_i(q_i) - \hat{\mu}_i(q_i)\big(-K_{\mathrm{P},i}\hat{y}_i + r_i\big) \\ -\hat{y}_{\mathrm{v},i} \end{bmatrix}}_{f_i^{\mathrm{v}}(x_i^{\mathrm{v}})} + \underbrace{\begin{bmatrix} 1 \\ 0 \end{bmatrix}}_{K_i^{\mathrm{v}}} d_i \tag{22a}$$

$$z_i = q_i. \tag{22b}$$

Moreover, (22) is EIP with supply rate $(z_i - \bar{z}_i)(d_i - \bar{d}_i)$ and positive definite storage function

$$H_i^{\mathrm{v}} = \tfrac{1}{2}\|x_i^{\mathrm{v}} - \bar{x}_i^{\mathrm{v}}\|^2_{\mathrm{diag}^{-1}(J_i, Q_{\mathrm{I},i})} \tag{23}$$

for any (feasible) equilibrium pair $(\bar{d}_i, \bar{z}_i)$ and associated equilibrium state

$$\bar{x}_i^{\mathrm{v}} = \begin{bmatrix} J_i q_i^* & Q_{\mathrm{I},i}\bar{r}_i \end{bmatrix}^\top \text{ or } \bar{x}_i^{\mathrm{v}} = \begin{bmatrix} 0 & Q_{\mathrm{I},i}\bar{r}_i \end{bmatrix}^\top. \tag{24}$$

Proof: See Appendix C.

Remark 9: The design of the PI controller (21) is based on the observation that the dynamics of a control valve in series with a pipe are EIP with respect to the (control) input–output pair $(u_{\mathrm{v},i}, \hat{y}_i)$. The definition of the output $\hat{y}_i$ originates from the fact that the input matrix $G_i(x_i)$ as in (6) is state-dependent. This circumstance complicates the use of a standard PI controller around the shifted passive output (see also [20], [32, p. 137], [44, p. 26]). Following [20, eq. (8)], we instead propose $\hat{y}_i$ as a new passive output, which is obtained from a suitable, *shifted* representation of the dynamics.

In steady state, $\hat{y}_i = 0$ generally allows for either $\bar{q}_i = q_i^*$ or $\bar{q}_i = 0$ [see (20) and (22)]. However, $\bar{q}_i = 0$ implies $\lambda_i(0) = 0$, $\hat{\mu}_i(0) = 0$ (see (2b) and Assumption 1), and, thus, $\bar{d}_i = 0$, where d_i is the pressure difference over the serial connection of valve and pipe element [see (6)]. This makes sense from a practical perspective, as a control valve with zero differential pressure cannot regulate is volume flow rate. Moreover, a positive pressure difference leads to a well-defined (desired) direction of the flow in the devices that are equipped with a control valve (i.e., $i \in \mathcal{D} \cup \mathcal{L} \cup \mathcal{M} \cup \mathcal{H}$). From a system design viewpoint, in practice, one can first identify via a steady-state analysis critical points corresponding to sections in the network with low pressure. Then, in order to achieve $d_i > 0$, booster pumps can be installed in such sections.

Assumption 4: Any control valve in series with a pipe element [see (6)] has a positive differential pressure $d_i > 0$ for all time. This implies for DGUs and consumer circuits $i \in \mathcal{D} \cup \mathcal{L}$ that $p_j + p_{\mathrm{P},i} - p_k > 0$ (see Figs. 6 and 7) and for mixing connections $i \in \mathcal{M}$ that $p_j - p_k > 0$ (see Fig. 8).

C. Properties of the Closed-Loop Systems

In this section, we deploy the controlled pumps and valves from Propositions 1–3 in the corresponding actuated edges and nodes $i \in \mathcal{D} \cup \mathcal{L} \cup \mathcal{P}_{\mathrm{boost}} \cup \mathcal{M} \cup \in \mathcal{H}$. In particular, we show that these closed-loop systems are also EIP, a fact which is central for the subsequent stability analysis of the overall, interconnected DHN model.

Lemma 1: Assign the pump controllers (10) and (15) and the valve controller (21) to the respective open-loop edge and node subsystems $i \in \mathcal{D} \cup \mathcal{L} \cup \mathcal{P}_{\mathrm{boost}} \cup \mathcal{M} \cup \mathcal{H}$ [see (4)–(6) and (8)] according to the control tasks in Problem 1. Then, the resulting closed-loop subsystems can be written as follows:

$$\dot{\hat{x}}_i = \hat{f}_i(\hat{x}_i) + \hat{K}_i d_i \tag{25a}$$

$$z_i = \hat{T}_i \hat{x}_i \tag{25b}$$

with appropriate vectors and matrices. Moreover, for any $i \in \mathcal{D} \cup \mathcal{L} \cup \mathcal{P}_{\mathrm{boost}} \cup \mathcal{M} \cup \mathcal{H}$, (25) is EIP with supply rate $(z_i - \bar{z}_i)(d_i - \bar{d}_i)$ and positive definite storage function

$$\hat{H}_i(\hat{x}_i, \bar{\hat{x}}_i) = \frac{1}{2}\|\hat{x}_i - \bar{\hat{x}}_i\|^2_{\hat{Q}_i} \tag{26}$$

where $\hat{\boldsymbol{Q}}_i$ is a suitable positive definite matrix and $\bar{\hat{\boldsymbol{x}}}_i$ is any (feasible) equilibrium value of $\hat{\boldsymbol{x}}_i$ associated with $\bar{d}_i$. In addition, under Assumption 4, the equilibrium value $\bar{\hat{\boldsymbol{x}}}_i$ of any $i \in \mathcal{D} \cup \mathcal{L} \cup \mathcal{P}_{\text{boost}} \cup \mathcal{M} \cup \mathcal{H}$ is such that $\bar{q}_i = q_i^*$ and $\bar{p}_{\text{P},i} = p_{\text{P},i}^*$ in accordance with Problem 1.

Proof: See Appendix D. ∎

Remark 10: Note that in Lemma 1 the original interaction input and output variables d_i and z_i are used. This is due to the fact that our control designs and the resulting closed-loop systems have not altered the description of the physical interconnection among the DHN subsystems.

VI. Modular Stability Analysis

In this section, we prove that any feasible, hydraulic equilibrium of the overall closed-loop DHN dynamics is asymptotically stable.

A. EIP of the Unactuated Edges and Nodes

First, we show that the unactuated pipe edges without booster pumps $i \in \mathcal{P} \setminus \mathcal{P}_{\text{boost}}$ and the capacitive nodes $i \in \mathcal{C}$ are EIP as well, although with nonassignable steady states.

Lemma 2: The model of any unactuated pipe edge (4) with $u_{\text{P},i} = 0$ and any capacitive node (9), i.e., any subsystem $i \in \mathcal{P} \setminus \mathcal{P}_{\text{boost}} \cup \mathcal{C}$, can be written as (25) with an appropriate choice of the defining vectors and matrices. Furthermore, these subsystems are EIP with some positive definite storage function in the form of (26).

Proof: See Appendix E. ∎

B. Interconnection Structure

Next, we illustrate the power-preserving nature of the interconnection structure between the edge and node subsystems of the DHN. In order to facilitate the subsequent elaborations and provide a compact representation, we assemble the overall system dynamics in vector form. Recall that the set of edges $\mathcal{E}$ is the ordered union of $\mathcal{D}$, $\mathcal{L}$, $\mathcal{P}$, and $\mathcal{M}$. Let Δ be the ordered union of the sets of nodes $\mathcal{H}$ and $\mathcal{C}$. For $\Omega = \{\mathcal{E}, \Delta\}$, let $\hat{\boldsymbol{x}}_\Omega = \text{stack}(\hat{\boldsymbol{x}}_i)_{i\in\Omega}$, $\hat{\boldsymbol{f}}_\Omega(\hat{\boldsymbol{x}}_\Omega) = \text{stack}(\hat{\boldsymbol{f}}_i(\hat{\boldsymbol{x}}_i))_{i\in\Omega}$, $\hat{\boldsymbol{K}}_\Omega = \text{diag}(\hat{\boldsymbol{K}}_i)_{i\in\Omega}$, $\boldsymbol{d}_\Omega = \text{stack}(d_i)_{i\in\Omega}$, $\boldsymbol{z}_\Omega = \text{stack}(z_i)_{i\in\Omega}$, $\hat{\boldsymbol{T}}_\Omega = \text{diag}(\hat{\boldsymbol{C}}_i)_{i\in\Omega}$, and $\hat{H}_\Omega(\hat{\boldsymbol{x}}_\Omega) = \sum_{i\in\Omega} \hat{H}_i(\hat{\boldsymbol{x}}_i)$, where for each $i \in \Omega$, $\hat{\boldsymbol{x}}_i$, $\hat{\boldsymbol{f}}_i$, $\hat{\boldsymbol{K}}_i$, d_i, z_i, and $\hat{H}_i$ are as in Lemmas 1 and 2. Then, the overall, closed-loop DHN can be written as follows:

$$\dot{\hat{\boldsymbol{x}}}_\mathcal{E} = \hat{\boldsymbol{f}}_\mathcal{E}(\hat{\boldsymbol{x}}_\mathcal{E}) + \hat{\boldsymbol{K}}_\mathcal{E}\boldsymbol{d}_\mathcal{E}, \;\; \boldsymbol{z}_\mathcal{E} = \hat{\boldsymbol{T}}_\mathcal{E}\hat{\boldsymbol{x}}_\mathcal{E} \tag{27a}$$

$$\dot{\hat{\boldsymbol{x}}}_\Delta = \hat{\boldsymbol{f}}_\Delta(\hat{\boldsymbol{x}}_\Delta) + \hat{\boldsymbol{K}}_\Delta\boldsymbol{d}_\Delta, \;\; \boldsymbol{z}_\Delta = \hat{\boldsymbol{T}}_\Delta\hat{\boldsymbol{x}}_\Delta \tag{27b}$$

$$0 = \hat{\boldsymbol{K}}_\mathcal{K}\boldsymbol{d}_\mathcal{K}. \tag{27c}$$

Let us denote by $\mathbb{B}$ the incidence matrix of the DHN digraph $\mathcal{G}$ (see Section II-A). With the considered ordering of the edges and nodes of $\mathcal{G}$, the incidence matrix can be written as follows:

$$\mathbb{B} = \begin{bmatrix} \mathbb{B}_{\Delta\mathcal{E}} \\ \mathbb{B}_{\mathcal{K}\mathcal{E}} \end{bmatrix}. \tag{28}$$

With (28), the interaction inputs of each of the subsystems in (27) can be represented as follows:

$$\boldsymbol{d}_\mathcal{E} = -\mathbb{B}_{\Delta\mathcal{E}}^\top \boldsymbol{z}_\Delta - \mathbb{B}_{\mathcal{K}\mathcal{E}}^\top \boldsymbol{z}_\mathcal{K} \tag{29a}$$

$$\boldsymbol{d}_\Delta = \mathbb{B}_{\Delta\mathcal{E}}\boldsymbol{z}_\mathcal{E} \tag{29b}$$

$$\boldsymbol{d}_\mathcal{K} = \mathbb{B}_{\mathcal{K}\mathcal{E}}\boldsymbol{z}_\mathcal{E}. \tag{29c}$$

Note, e.g., that for any $i \in \mathcal{E}$, $d_i = p_j - p_k$, where $(j,k) \in \mathcal{N}_i^- \times \mathcal{N}_i^+$ [see (5)]. That is, d_i is expressed as the product of an appropriate column of $\mathbb{B}$ and the vector $[\boldsymbol{z}_\Delta^\top \; \boldsymbol{z}_\mathcal{K}^\top]^\top$. Subsequently, we can establish the following lemma, which will be useful later to analyze the stability of (27).

Lemma 3: The interconnection structure (29) among the subsystems in (27) is power-preserving.

Proof: As (29) is a skew-symmetric interconnection structure, it holds for all time that

$$\boldsymbol{z}_\mathcal{E}^\top\boldsymbol{d}_\mathcal{E} + \boldsymbol{z}_\Delta^\top\boldsymbol{d}_\Delta + \boldsymbol{z}_\mathcal{K}^\top\boldsymbol{d}_\mathcal{K} = 0. \tag{30}$$

Hence, the interconnection among the subsystems in (27) is power-preserving.[6] ∎

The system conformed by (27)–(29) is an index-2 differential algebraic system in Hessenberg form (see [47]). Based on [47], the time derivative of the algebraic constraint (27c) can be computed once to explicitly obtain $\boldsymbol{z}_\mathcal{K}$ in terms of $\hat{\boldsymbol{x}}_\mathcal{E}$ and $\hat{\boldsymbol{x}}_\Delta$ as follows:

$$\begin{aligned} &\boldsymbol{z}_\mathcal{K} = \Phi(\hat{\boldsymbol{x}}_\mathcal{E}, \hat{\boldsymbol{x}}_\Delta) \\ &\Phi := \left(\mathbb{B}_{\mathcal{K}\mathcal{E}}\text{diag}\left(\tfrac{1}{J_i}\right)_{i\in\mathcal{E}}\mathbb{B}_{\mathcal{K}\mathcal{E}}^\top\right)^{-1}\left(\hat{\boldsymbol{K}}_\mathcal{E}\mathbb{B}_{\Delta\mathcal{E}}^\top\hat{\boldsymbol{C}}_\Delta\hat{x}_\Delta - \hat{\boldsymbol{f}}_\mathcal{E}(\hat{\boldsymbol{x}}_\mathcal{E})\right) \end{aligned} \tag{31}$$

where we have used the fact that $\hat{\boldsymbol{K}}_\mathcal{K}$ is an identity matrix and $\hat{\boldsymbol{C}}_\mathcal{E}\hat{\boldsymbol{K}}_\mathcal{E} = \text{diag}(1/J_i)_{i\in\mathcal{E}}$. Then, (27)–(29) are equivalent to the ordinary differential equations (ODEs)

$$\dot{\hat{\boldsymbol{x}}}_\mathcal{E} = \hat{\boldsymbol{f}}_\mathcal{E}(\hat{\boldsymbol{x}}_\mathcal{E}) - \hat{\boldsymbol{K}}_\mathcal{E}\mathbb{B}_{\Delta\mathcal{E}}^\top\hat{\boldsymbol{T}}_\Delta\hat{\boldsymbol{x}}_\Delta - \hat{\boldsymbol{K}}_\mathcal{E}\mathbb{B}_{\mathcal{K}\mathcal{E}}^\top\Phi(\hat{\boldsymbol{x}}_\mathcal{E}, \hat{\boldsymbol{x}}_\Delta) \tag{32a}$$

$$\dot{\hat{\boldsymbol{x}}}_\Delta = \hat{\boldsymbol{f}}_\Delta(\hat{\boldsymbol{x}}_\Delta) + \hat{\boldsymbol{K}}_\Delta\mathbb{B}_{\Delta\mathcal{E}}\hat{\boldsymbol{C}}_\mathcal{E}\hat{\boldsymbol{x}}_\mathcal{E} \tag{32b}$$

defined on the invariant manifold

$$\mathbb{M} = \left\{(\hat{\boldsymbol{x}}_\mathcal{E}, \hat{\boldsymbol{x}}_\Delta) : \; 0 = \hat{\boldsymbol{K}}_\mathcal{K}\mathbb{B}_{\mathcal{K}\mathcal{E}}\hat{\boldsymbol{C}}_\mathcal{E}\hat{\boldsymbol{x}}_\mathcal{E}\right\}. \tag{33}$$

The positive definiteness and invertibility of $\mathbb{B}_{\mathcal{K}\mathcal{E}}\text{diag}(1/J_i)_{i\in\mathcal{E}}\mathbb{B}_{\mathcal{K}\mathcal{E}}^\top$ in (31) follow from the fact that $\mathbb{B}_{\mathcal{K}\mathcal{E}}\mathbb{B}_{\mathcal{K}\mathcal{E}}^\top$ is a principal submatrix of the Laplacian $\mathbb{L} = \mathbb{B}\mathbb{B}^\top$ of the DHN graph. This submatrix is invariant under removal of any row of $\mathbb{B}$ not associated with $\mathcal{K}$. Removal of any such row can be understood as a *grounding* of $\mathcal{G}$ (see [48] for a definition). Laplacians of grounded connected graphs, or grounded Laplacians, are positive definite [48]. Note directly that $\mathbb{B}_{\mathcal{K}\mathcal{E}}\Theta\mathbb{B}_{\mathcal{K}\mathcal{E}}^\top$ is positive definite for any symmetric, positive definite matrix Θ.

C. Asymptotic Stability of the Hydraulic DHN Equilibrium

As a last step, we combine the EIP properties of the DHN subsystems analyzed in Lemmas 1 and 2, the power-preserving property of their interconnection structure shown in Lemma 3, and LaSalle's invariance principle to prove asymptotic stability of any feasible, hydraulic DHN equilibrium in a modular, bottom-up manner.

[6]The equivalence (30) also holds if the respective (interaction) input–output pairs are shifted with respect to any feasible equilibrium values.

TABLE I
PRESSURE AND VOLUME FLOW RATE SET POINTS

Edges		$p^*_{\mathrm{P},i}$ in 10^5 Pa	q^*_i in 10^{-3} m^3/s
DGU 1		15	—
DGU 2		10	3.5 (4.5)
DGU 3		—	3
Consumer 4		—	2
Consumer 5		—	2
Consumer 6		—	2 (4)
Consumer 7		6	2.5 (5)
Consumer 8		—	3 (6)
Pipe 15		5	—
Mix. Connection 25		—	1 (3)
Nodes			
Pressure holding 4		2	—

Theorem 1: Consider a DHN with arbitrary setup as described in Sections II and III in which pumps and valves are controlled as in Lemma 1. Then, under Assumptions 3 and 4, any feasible hydraulic equilibrium $(\hat{x}_{\mathcal{E}}, \hat{x}_{\Delta})$ of such a DHN is asymptotically stable. Furthermore, the pump pressures as well as the pump and valve volume flow rates take on the steady states specified in Problem 1, i.e., for any $i \in \mathcal{D} \cup \mathcal{L} \cup \mathcal{P}_{\mathrm{boost}} \cup \mathcal{M} \cup \mathcal{H}$, the respective $\hat{x}_i$ in $(\hat{x}_{\mathcal{E}}, \hat{x}_{\Delta})$ is such that $\bar{q}_i = \bar{q}_{\mathrm{P},i} = q^*_i$ and $\bar{p}_{\mathrm{P},i} = p^*_{\mathrm{P},i}$ in accordance with Problem 1.

Proof: See Appendix F.

VII. SIMULATION

In this section, we demonstrate the stabilizing properties, plug-and-play capabilities, and robustness of the proposed pressure and volume flow rate controllers via simulations in MATLAB/SIMULINK using SIMSCAPE components. In Section VII-A, we present a scenario with plug-and-play operations and varying reference values. In Section VII-B, the first scenario is repeated, albeit with parameter uncertainties and a saturation to the valve input.

The simulations are conducted by means of the DHN depicted in Fig. 1, which shows all structural features discussed in Sections II and III. Furthermore, we cover all control problems outlined in Problem 1 by assigning appropriate DGU, consumer, and pressure holding configurations, i.e., $\mathcal{D}_{\mathrm{form}} = \{1\}$, $\mathcal{D}_{\mathrm{valve}} = \{2\}$, $\mathcal{D}_{\mathrm{VSP}} = \{3\}$, $\mathcal{L}_{\mathrm{boost}} = \{7\}$, $\mathcal{L}_{\mathrm{valve}} = \{4, 5, 6\}$, $\mathcal{L}_{\mathrm{VSP}} = \{8\}$, $\mathcal{P}_{\mathrm{boost}} = \{15\}$, $\mathcal{M} = \{25\}$, and $\mathcal{H} = \{4\}$.

The model and controller parameters used in the simulations are reported in [1, Tables I and II].

A. Scenario A: Plug-and-Play and Set-Point Changes

In this scenario, the simulation starts with DGU 3 disconnected. The pressure and volume flow rate set points for the pumps and valves are assigned as in Table I. At the indicated times, the following events occur.

1) $t = 5$ s*:* Consumers $i \in \{6, 7, 8\}$ increase their volume flow rates by 100 % until $t = 10$ s.
2) $t = 20$ s*:* To help cover the increased demand, DGU 3 connects, and the mixing connection 25 increases its volume flow rate to 3×10^{-3} m^3/s.
3) $t = 30$ s*:* DGU 2 increases its input volume flow rate to 4.5×10^{-3} m^3/s.
4) $t = 40$ s*:* Consumer 4 disconnects.

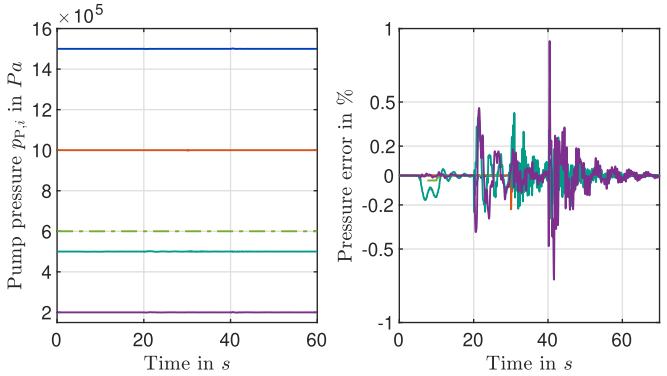

Fig. 9. Scenario A: simulated pump pressures in DGUs $i \in \{1, 2\}$, consumer $i \in \{7\}$, booster pump $i \in \{15\}$, and dynamic pressure holding unit at node $j \in \{4\}$ with corresponding deviations from the references; the line colors are as per Table I.

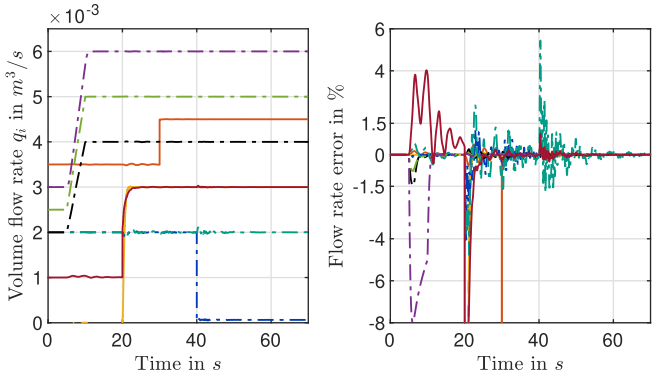

Fig. 10. Scenario A: simulated volume flow rates through DGUs $i \in \{2, 3\}$, consumers $i \in \{4, 5, 6, 7, 8\}$, and mixing valve $i \in \{25\}$ with corresponding deviations from the references; the line colors are as per Table I.

The pressure and volume flow rate trajectories shown in Figs. 9 and 10 confirm the theoretical stability statements. Despite plug-and-play operations and changing operating conditions, the pressures of pressure-controlled pumps and the volume flow rates of flow-controlled pumps and valves are asymptotically stabilized at their desired set points. For the pressures, the maximum deviations resulting from the events at $t = 5$, 20, 30, and 40 s remain within a 1 % band with respect to the set points and subside below 0.2 % within approximately 5 s. For the volume flow rates, larger deviations can be observed. In particular at $t = 20$ s and $t = 30$ s during the connection of DGU 3, the set point that changes the error plots in Fig. 10 shows large outliers. However, from a practical perspective, this is natural as abrupt set point changes cannot be realized instantly by the respective volume flow rate controllers. More importantly, except for the load ramps at $t \in [5, 10]$ s, the volume flow rates settle to within a 1.5 % band with respect to the set points after at most 5 s. During the load ramps, the errors are slightly higher, but remain below 8 %. This shows that the volume flow rate controllers for both pumps and valves, although not specifically designed

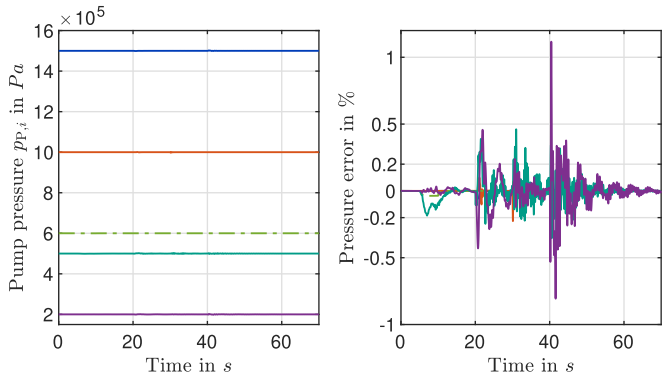

Fig. 11. Scenario B: simulated pump pressures in DGUs $i \in \{1, 2\}$, consumer $i \in \{7\}$, booster pump $i \in \{15\}$, and dynamic pressure holding unit at node $j \in \{4\}$ with corresponding deviations from the references; the line colors are as per Table I.

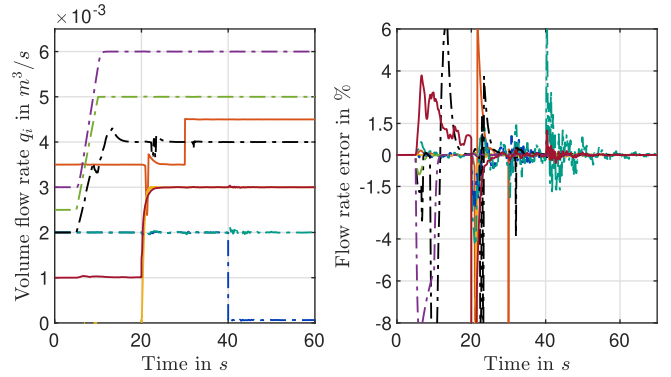

Fig. 12. Scenario B: simulated volume flow rates through DGUs $i \in \{2, 3\}$, consumers $i \in \{4, 5, 6, 7, 8\}$, and mixing valve $i \in \{25\}$ with corresponding deviations from the references; the line colors are as per Table I.

for it, are sufficiently fast to adquately track set points that vary on a time scale of seconds.

B. Scenario B: Parameter Uncertainty and Valve Saturation

Scenario B is similar to Scenario A except for two modification: first, a 10 % uncertainty is added to the pump parameters $R_{\mathrm{P},i}$, $J_{\mathrm{P},i}$, and $C_{\mathrm{P},i}$ and the valve parameters $C_{\mathrm{v},i}$; second, the virtual valve control input of all valves is saturated to $u_{\mathrm{v}} \in [1, u_{\mathrm{v},i}^{\max}]$ (see Assumption 2).[7]

The resulting pressure and volume flow rate trajectories shown in Figs. 11 and 12 are similar to those shown in Fig. 9. The main difference introduced by the valve saturation is an impaired convergence performance of the volume flow rate control via valves, particularly at DGU 2 and Consumer 6 (see the orange and black lines in Fig. 12). In practice, an appropriate redesign of the valves or by increasing the available pressure, e.g., via the booster pump in Pipe 15 or a separate booster pump in the respective consumer, the control performance can be improved.

Overall, the results of the two scenarios illustrate that the passivity-based pressure and volume flow rate controllers indeed asymptotically stabilize the hydraulic variables while allowing for plug-and-play operations of the different DHN subsystems. Furthermore, the integral parts of the proposed controllers ensure zero steady-state errors in the presence of parameter uncertainties and changing hydraulic conditions naturally occurring during the operation of DHNs.

[7]In line with classical feedback control design, we did not consider the possibility of control input saturation explicitly during the control design stage in Section V. Instead, we analyze its impact by means of the numerical simulation in this section.

VIII. Conclusion

In this work, we have proposed a unifying control framework that guarantees asymptotic pressure and volume flow rate stability based on the EIP properties of the DHN subsystem models. We provided a comprehensive hydraulic model covering state of the art as well as future DHN generations and formalized the hydraulic control problems arising in such systems. Subsequently, we designed decentralized, passivity-based controllers for the pumps and valves in the DHN subsystems and proposed three controllers: two for pressure and volume flow rate control via pumps and one for volume flow rate control via valves. Based on the EIP properties of the (actuated and unactuated) subsystem models, the skew-symmetry of their interconnection structure, and LaSalle's invariance principle, we then proved asymptotic stability of any feasible, hydraulic DHN equilibrium in a modular manner. In conclusion, we want to highlight that the modular approach of the EIP-based stability analysis allows to incorporate different and more detailed models (e.g., for the pumps and valves) and presents general guidelines for developing other decentralized pressure and volume flow rate controllers.

Appendix A
Proof of Proposition 1

Following [19], we begin by introducing a change of coordinates from $q_{\mathrm{P},i}$ to χ_i as follows [see (10b)]:

$$\chi_i = q_{\mathrm{P},i} + r_i. \tag{34}$$

Then, by computing $\dot{\chi}_i$, we get

$$J_{\mathrm{P},i}\dot{\chi}_i = J_{\mathrm{P},i}\dot{q}_{\mathrm{P},i} + J_{\mathrm{P},i}\dot{r}_i = \nu_i + u_{\mathrm{P},i} \tag{35}$$

where ν_i is given in (10c). Following the IDA-PBC design methodology [18], we assign $u_{\mathrm{P},i}$ as in (10d) to obtain

$$J_{\mathrm{P},i}\dot{\chi}_i = -R_i^{\mathrm{p}}\chi_i - \left(p_{\mathrm{P},i} - p_{\mathrm{P},i}^{*}\right). \tag{36}$$

By propagating the coordinate transformation (34) to the $p_{\mathrm{P},i}$ dynamics, we can write the closed-loop dynamics as in (11). In order to show that (11) is EIP with supply rate $(d_i - \bar{d}_i)(z_i - \bar{z}_i)$ and positive definite storage function H_i^{p} in (12), let $\bar{d}_i$ denote an arbitrary equilibrium value of d_i with associated equilibria $\bar{z}_i$ for the output and $\bar{\boldsymbol{x}}_i^{\mathrm{p}}$ [see (13)] for the state vector. Since $\bar{\boldsymbol{x}}_i^{\mathrm{p}}$ satisfies $\boldsymbol{f}_i^{\mathrm{p}}(\bar{\boldsymbol{x}}_i^{\mathrm{p}}) + \boldsymbol{K}_i^{\mathrm{p}}\bar{d}_i = 0$, we can write (11) equivalently as follows:

$$\dot{\boldsymbol{x}}_i^{\mathrm{p}} = \boldsymbol{f}_i^{\mathrm{p}}(\boldsymbol{x}_i^{\mathrm{p}}) - \boldsymbol{f}_i^{\mathrm{p}}\left(\bar{\boldsymbol{x}}_i^{\mathrm{p}}\right) + \boldsymbol{K}_i^{\mathrm{p}}(d_i - \bar{d}_i). \tag{37}$$

For the time derivative of H_i^{p} in (12), it holds that

$$\dot{H}_i^{\mathrm{p}} = \nabla^{\top} H_i^{\mathrm{p}}\dot{\boldsymbol{x}}_i^{\mathrm{p}} = -\psi_i^{\mathrm{p}}(\boldsymbol{x}_i^{\mathrm{p}}) + (z_i - \bar{z}_i)(d_i - \bar{d}_i) \tag{38a}$$

$$\psi_i^{\mathrm{p}}(\boldsymbol{x}_i^{\mathrm{p}}) = R_i^{\mathrm{p}}(\chi_i - \bar{\chi}_i)^2 \tag{38b}$$

where we have used the identity

$$(\boldsymbol{K}_i^{\mathrm{p}})^\top \nabla H_i^{\mathrm{p}} = z_i - \bar{z}_i = p_{\mathrm{P},i} - \bar{p}_{\mathrm{P},i}.$$

Since $R_i^{\mathrm{p}} > 0$, it follows that $\psi_i^{\mathrm{p}}(\boldsymbol{x}_i^{\mathrm{p}}) \geq 0$, implying $\dot{H}_i^{\mathrm{p}} \leq (z_i - \bar{z}_i)(d_i - \bar{d}_i)$. Hence, EIP is established.

Appendix B
Proof of Proposition 2

By combining (4) with controller (15), the closed-loop system (17) follows directly. In order to show that system (17) is EIP with supply rate $(d_i - \bar{d}_i)(z_i - \bar{z}_i)$ and positive definite storage function H_i^{f} in (18), let $\bar{d}_i$ denote an arbitrary equilibrium value of d_i with associated equilibria $\bar{z}_i$ for the output and $\bar{\boldsymbol{x}}_i^{\mathrm{f}}$ [see (19)] for the state vector. Since $\bar{\boldsymbol{x}}_i^{\mathrm{f}}$ satisfies $\boldsymbol{f}_i^{\mathrm{f}}(\bar{\boldsymbol{x}}_i^{\mathrm{f}}) + \boldsymbol{K}_i^{\mathrm{f}} \bar{d}_i = 0$, we can write (17a) equivalently as follows:

$$\dot{\boldsymbol{x}}_i^{\mathrm{f}} = \boldsymbol{f}_i^{\mathrm{f}}(\boldsymbol{x}_i^{\mathrm{f}}) - \boldsymbol{f}_i^{\mathrm{f}}\left(\bar{\boldsymbol{x}}_i^{\mathrm{f}}\right) + \boldsymbol{K}_i^{\mathrm{f}}(d_i - \bar{d}_i). \tag{39}$$

For the time derivative of H_i^{f} in (18), it holds that

$$\dot{H}_i^{\mathrm{f}} = \nabla^\top H_i^{\mathrm{f}} \dot{\boldsymbol{x}}^{\mathrm{f}} = -\psi_i^{\mathrm{f}}(\boldsymbol{x}_i^{\mathrm{f}}) + (z_i - \bar{z}_i)(d_i - \bar{d}_i) \tag{40a}$$

$$\psi_i^{\mathrm{f}}(\boldsymbol{x}_i^{\mathrm{f}}) = (q_i - \bar{q}_i)\big(\lambda_i(q_i) - \lambda_i(\bar{q}_i)\big) + 2\frac{R_{\mathrm{P},i} Q_{\mathrm{I},i}}{\kappa_i^{\mathrm{f}}}\left(q_{\mathrm{P},i} - \bar{q}_{\mathrm{P},i}\right)^2 \tag{40b}$$

where we have used the identity

$$(\boldsymbol{K}_i^{\mathrm{f}})^\top \nabla H_i^{\mathrm{f}} = z_i - \bar{z}_i = q_i - \bar{q}_i.$$

Since $\lambda_i(q_i)$ is strictly increasing and (16) holds, it follows that $\psi_i^{\mathrm{f}}(\boldsymbol{x}_i^{\mathrm{f}}) \geq 0$, implying $\dot{H}_i^{\mathrm{f}} \leq (z_i - \bar{z}_i)(d_i - \bar{d}_i)$. Hence, EIP is established.

Appendix C
Proof of Proposition 3

Following the same reasoning as in the proof of Proposition 2 together with using $\bar{u}_i = \bar{r}_i$ and adding and subtracting $\hat{\mu}_i(q_i)\bar{r}_i$, we can write the closed-loop system (22) equivalently as follows:

$$J_i \dot{q}_i = -\big(\lambda_i(q_i) - \lambda_i(\bar{q}_i)\big) + \hat{\mu}_i(q_i) K_{\mathrm{P},i} \hat{y}_i - \hat{\mu}_i(q_i)(r_i - \bar{r}_i) - \bar{r}_i\big(\hat{\mu}_i(q_i) - \hat{\mu}_i(\bar{q}_i)\big) + (d_i - \bar{d}_i) \tag{41a}$$

$$Q_{\mathrm{I},i} \dot{r}_i = \hat{\mu}_i(q_i)(q_i - q_i^*). \tag{41b}$$

Note that (41) is equivalent to

$$\dot{\boldsymbol{x}}_i^{\mathrm{v}} = \boldsymbol{f}_i^{\mathrm{v}}(\boldsymbol{x}_i^{\mathrm{v}}) - \boldsymbol{f}_i^{\mathrm{v}}(\bar{x}_i^{\mathrm{v}}) + \boldsymbol{K}_i^{\mathrm{v}}(d_i - \bar{d}_i) \tag{42}$$

for any arbitrary equilibrium pair $(\bar{d}_i, \bar{z}_i)$ and associated equilibrium state vector $\bar{\boldsymbol{x}}_i^{\mathrm{v}}$ [see (24)]. For the time derivative of H_i^{v} in (23), it holds that

$$\dot{H}_i^{\mathrm{v}} = \nabla^\top H_i^{\mathrm{v}} \dot{\boldsymbol{x}}_i^{\mathrm{v}} = -\psi^{\mathrm{v}}(\boldsymbol{x}_i^{\mathrm{v}}) + (z_i - \bar{z}_i)(d_i - \bar{d}_i) \tag{43}$$

$$\psi_i^{\mathrm{v}}(\boldsymbol{x}_i^{\mathrm{v}}) = (q_i - \bar{q}_i)\big(\lambda_i(q_i) - \lambda_i(\bar{q}_i)\big) + K_{\mathrm{P},i}\hat{y}_i^2 + \bar{r}_i(q_i - \bar{q}_i)\big(\hat{\mu}_i(q_i) - \hat{\mu}_i(\bar{q}_i)\big) \tag{44}$$

where we have used the identity

$$(\boldsymbol{K}_i^{\mathrm{v}})^\top \nabla H_i^{\mathrm{v}} = z_i - \bar{z}_i = q_i - \bar{q}_i.$$

Since both $\lambda_i(q_i)$ and $\hat{\mu}_i(q_i)$ are strictly increasing [see Assumption 1 and (2b)], $\bar{u}_i = \bar{r}_i > 0$ per definition (see Section III-A2), and $K_{\mathrm{P},i} > 0$, it follows that $\psi_i^{\mathrm{v}}(\boldsymbol{x}_i^{\mathrm{v}}) \geq 0$, implying $\dot{H}_i^{\mathrm{v}} \leq (z_i - \bar{z}_i)(d_i - \bar{d}_i)$. Hence, EIP is established.

Appendix D
Proof of Lemma 1

In the following, we consider the closed-loop systems according to their order from 1)–5) in Problem 1. Thus, we begin with $i \in \mathcal{D}_{\mathrm{form}}$. By combining the open-loop DGU model (5) with $u_{\mathrm{P},i}$ in (10d) and fixing $u_{\mathrm{v},i} = \bar{u}_{\mathrm{v},i} > 0$ (due to $s_{\mathrm{v},i} = 1$), we can write the closed-loop system as in (25), i.e.,

$$\frac{\mathrm{d}}{\mathrm{d}t}\underbrace{\begin{bmatrix} J_i q_i \\ J_{\mathrm{P},i}\chi_i \\ C_{\mathrm{P},i} p_{\mathrm{P},i} \\ Q_{\mathrm{I},i} r_i \end{bmatrix}}_{\hat{\boldsymbol{x}}_i} = \underbrace{\begin{bmatrix} p_{\mathrm{P},i} - \lambda_i(q_i) - \hat{\mu}_i(q_i)\bar{u}_{\mathrm{v},i} \\ -R_i^{\mathrm{p}}\chi_i - \left(p_{\mathrm{P},i} - p_{\mathrm{P},i}^*\right) \\ \chi_i - r_i \\ \left(p_{\mathrm{P},i} - p_{\mathrm{P},i}^*\right) \end{bmatrix}}_{\hat{f}_i(\hat{\boldsymbol{x}}_i)} + \underbrace{\begin{bmatrix} 1 \\ 0 \\ 0 \\ 0 \end{bmatrix}}_{\hat{\boldsymbol{K}}_i} d_i \tag{45a}$$

$$z_i = \underbrace{\begin{bmatrix} \frac{1}{J_i} & 0 & 0 & 0 \end{bmatrix}}_{\hat{\boldsymbol{T}}_i} \hat{\boldsymbol{x}}_i \tag{45b}$$

with d_i as in (5). To show that (45) is EIP, we follow the same reasoning as in the proofs of Propositions 1 and 2. The storage function $\hat{H}_i$ is as in (26) with

$$\hat{\boldsymbol{Q}}_i = \mathrm{diag}^{-1}\left(J_i, J_{\mathrm{P},i}, C_{\mathrm{P},i}, Q_{\mathrm{I},i}\right). \tag{46}$$

The time derivative of $\hat{H}_i$ along the solutions of (45) satisfies

$$\dot{\hat{H}}_i = \nabla^\top \hat{H}_i \dot{\hat{\boldsymbol{x}}}_i = -\hat{\psi}_i(\hat{\boldsymbol{x}}_i) + (z_i - \bar{z}_i)(d_i - \bar{d}_i) \tag{47}$$

$$\hat{\psi}_i(\hat{\boldsymbol{x}}_i) = (q_i - \bar{q}_i)\big(\lambda_i(q_i) - \lambda_i(\bar{q}_i)\big) + R_i^{\mathrm{P}}\left(\chi_i - \bar{\chi}_i\right)^2 + (q_i - \bar{q}_i)\bar{u}_{\mathrm{v},i}\big(\hat{\mu}_i(q_i) - \hat{\mu}(\bar{q}_i)\big) \tag{48}$$

where we have used the identity

$$\hat{\boldsymbol{K}}_i^\top \nabla \hat{H}_i = z_i - \bar{z}_i = q_i - \bar{q}_i = \hat{\boldsymbol{T}}_i(\hat{\boldsymbol{x}}_i - \bar{\hat{x}}_i).$$

As λ_i and $\hat{\mu}_i$ are strictly increasing and $\bar{u}_{\mathrm{v},i}, R_i^{\mathrm{P}} > 0$, it follows that $\hat{\psi}_i(\hat{\boldsymbol{x}}_i) \geq 0$ and $\dot{\hat{H}}_i \leq (z_i - \bar{z}_i)(d_i - \bar{d}_i)$. Hence, (45) is EIP. Finally, observe that due to the integral action (10a), it holds for any feasible equilibrium value of $\hat{\boldsymbol{x}}_i$ that $\bar{p}_{\mathrm{P},i} = p_{\mathrm{P},i}^*$.

Next, we consider $i \in \mathcal{D}_{\mathrm{valve}}$. By combining the open-loop DGU model (5) with $u_{\mathrm{P},i}$ and $u_{\mathrm{v},i}$ in (10d) and (21b), respectively, we can write the closed-loop system as in (25), i.e.,

$$\frac{\mathrm{d}}{\mathrm{d}t}\underbrace{\begin{bmatrix} J_i q_i \\ J_{\mathrm{P},i}\chi_i \\ C_{\mathrm{P},i} p_{\mathrm{P},i} \\ Q_{\mathrm{I},i}^{\alpha} r_i^{\alpha} \\ Q_{\mathrm{I},i}^{\beta} r_i^{\beta} \end{bmatrix}}_{\hat{\boldsymbol{x}}_i} = \underbrace{\begin{bmatrix} p_{\mathrm{P},i} - \lambda_i(q_i) - \hat{\mu}_i(q_i)\left(-K_{\mathrm{P},i}\hat{y}_i + r_i^{\beta}\right) \\ -R_i^{\mathrm{p}}\chi_i - \left(p_{\mathrm{P},i} - p_{\mathrm{P},i}^*\right) \\ \chi_i - r_i^{\alpha} \\ \left(p_{\mathrm{P},i} - p_{\mathrm{P},i}^*\right) \\ \hat{\mu}_i(q_i)\left(q_i - q_i^*\right) \end{bmatrix}}_{\hat{f}_i(\hat{\boldsymbol{x}}_i)} + \underbrace{\begin{bmatrix} 1 \\ 0 \\ 0 \\ 0 \\ 0 \end{bmatrix}}_{\hat{\boldsymbol{K}}_i} d_i \tag{49a}$$

$$z_i = \underbrace{\begin{bmatrix} \frac{1}{J_i} & 0 & 0 & 0 & 0 \end{bmatrix}}_{\hat{\boldsymbol{T}}_i} \hat{\boldsymbol{x}}_i \tag{49b}$$

with d_i as in (5). Note that we have used the indices α and β to distinguish between the integral actions of (10) and (21), respectively. To show that (49) is EIP, we proceed as before. The storage function $\hat{H}_i$ is as in (26) with

$$\hat{\boldsymbol{Q}}_i = \operatorname{diag}^{-1}\Big(J_i,\, J_{\mathrm{P},i},\, C_{\mathrm{P},i},\, Q^{\alpha}_{\mathrm{I},i},\, Q^{\beta}_{\mathrm{I},i}\Big). \tag{50}$$

The time derivative of $\hat{H}_i$ along the solutions of (49) satisfies

$$\dot{\hat{H}}_i = \nabla^\top \hat{H}_i \dot{\hat{x}}_i = -\hat{\psi}_i(\hat{x}_i) + (z_i - \bar{z}_i)(d_i - \bar{d}_i) \tag{51}$$

$$\begin{aligned}\hat{\psi}_i(\hat{\boldsymbol{x}}_i) &= (q_i - \bar{q}_i)\big(\lambda_i(q_i) - \lambda_i(\bar{q}_i)\big) + R^{\mathrm{P}}_i(\chi_i - \bar{\chi}_i)^2 \\ &\quad + \bar{r}^{\beta}_i(q_i - \bar{q}_i)\big(\hat{\mu}_i(q_i) - \hat{\mu}_i(\bar{q}_i)\big) + K_{\mathrm{P},i}\hat{y}_i^2\end{aligned} \tag{52}$$

where we have used the identity

$$\hat{\boldsymbol{K}}_i^\top \nabla \hat{H}_i = z_i - \bar{z}_i = q_i - \bar{q}_i = \hat{\boldsymbol{T}}_i(\hat{\boldsymbol{x}}_i - \bar{\hat{x}}_i).$$

With the same reasoning as for (44) and considering that $R^{\mathrm{P}}_i > 0$, it follows that $\hat{\psi}_i(\hat{\boldsymbol{x}}_i) \geq 0$ and $\dot{\hat{H}}_i \leq (z_i - \bar{z}_i)(d_i - \bar{d}_i)$. Hence, EIP is established. Finally, observe that due to the integral actions (10a) and (21a) and Assumption 4, it holds for any feasible equilibrium value of $\hat{\boldsymbol{x}}_i$ that $\bar{q}_i = q_i^*$ and $\bar{p}_{\mathrm{P},i} = p^*_{\mathrm{P},i}$.

For $i \in \mathcal{D}_{\mathrm{VSP}}$, we combine the open-loop DGU model (5) with $u_{\mathrm{P},i}$ as in (15b) and fix $u_{\mathrm{v},i} = \bar{u}_{\mathrm{v},i} > 0$ (due to $s_{\mathrm{v},i} = 1$) to write the closed-loop system as in (25), i.e.,

$$\underbrace{\frac{\mathrm{d}}{\mathrm{d}t}\begin{bmatrix} J_i q_i \\ J_{\mathrm{P},i} q_{\mathrm{P},i} \\ C_{\mathrm{P},i}\, p_{\mathrm{P},i} \\ Q_{\mathrm{I},i} r_i \end{bmatrix}}_{\dot{\hat{\boldsymbol{x}}}_i} = \underbrace{\begin{bmatrix} p_{\mathrm{P},i} - \lambda_i(q_i) - \hat{\mu}_i(q_i)\bar{u}_{\mathrm{v},i} \\ -p_{\mathrm{P},i} - R_{\mathrm{P},i} q_{\mathrm{P},i} - K_{\mathrm{P},i}\, p_{\mathrm{P},i} - r_i \\ q_{\mathrm{P},i} - q_i \\ (q_i - q_i^*) \end{bmatrix}}_{\hat{f}_i(\hat{\boldsymbol{x}}_i)} + \underbrace{\begin{bmatrix} 1 \\ 0 \\ 0 \\ 0 \end{bmatrix}}_{\hat{\boldsymbol{K}}_i} d_i \tag{53a}$$

$$z_i = \underbrace{\begin{bmatrix} \frac{1}{J_i} & 0 & 0 & 0 \end{bmatrix}}_{\hat{\boldsymbol{T}}_i} \hat{\boldsymbol{x}}_i \tag{53b}$$

with d_i as in (5). To show that (53) is EIP, we note that $\hat{H}_i$ is given by (26) with $\hat{\boldsymbol{Q}}_i = \boldsymbol{Q}_i^{\mathrm{f}}$ from (18b). The time derivative of $\hat{H}_i$ along the solutions of (53) satisfies

$$\dot{\hat{H}}_i = \nabla^\top \hat{H}_i \dot{\hat{x}}_i = -\hat{\psi}_i(\hat{x}_i) + (z_i - \bar{z}_i)(d_i - \bar{d}_i) \tag{54}$$

$$\begin{aligned}\hat{\psi}_i(\hat{\boldsymbol{x}}_i) &= (q_i - \bar{q}_i)\big(\lambda_i(q_i) - \lambda_i(\bar{q}_i)\big) \\ &\quad + (q_i - \bar{q}_i)\bar{u}_{\mathrm{v},i}\big(\hat{\mu}_i(q_i) - \hat{\mu}(\bar{q}_i)\big) \\ &\quad + 2\frac{R_{\mathrm{P},i} Q_{\mathrm{I},i}}{\kappa_i^{\mathrm{f}}}(q_{\mathrm{P},i} - \bar{q}_{\mathrm{P},i})^2\end{aligned} \tag{55}$$

where we have used the identity

$$\hat{\boldsymbol{K}}_i^\top \nabla \hat{H}_i = z_i - \bar{z}_i = q_i - \bar{q}_i = \hat{\boldsymbol{T}}_i(\hat{\boldsymbol{x}}_i - \bar{\hat{x}}_i).$$

As λ_i and $\hat{\mu}_i$ are strictly increasing, $\bar{u}_{\mathrm{v},i} > 0$, and (16) holds, it follows that $\hat{\psi}_i(\hat{\boldsymbol{x}}_i) \geq 0$ and $\dot{\hat{H}}_i \leq (z_i - \bar{z}_i)(d_i - \bar{d}_i)$. Hence, (53) is EIP. Finally, observe that due to the integral action (15a), it holds for any feasible equilibrium value of $\hat{\boldsymbol{x}}_i$ that $\bar{q}_i = \bar{q}_{\mathrm{P},i} = q_i^*$.

For describing the consumers $\mathcal{L}$ in closed loop, we recall that the open-loop model of any $i \in \mathcal{L}$ is identical to that of any DGU $i \in \mathcal{D}$, i.e., to (5). For $i \in \mathcal{L}_{\mathrm{boost}}$, we assign $u_{\mathrm{P},i}$ and $u_{\mathrm{v},i}$ as in (10d) and (21b), respectively. Then, the resulting closed-loop system is equivalent to (49) with the same EIP and equilibrium properties. Next, we consider $i \in \mathcal{L}_{\mathrm{valve}}$. In this case, the associated pump can either be turned off or is not present. Thus, the open loop of any $i \in \mathcal{L}_{\mathrm{valve}}$ is equivalent to that of a control valve in series with a pipe element, i.e., (6). By closing the loop with $u_{\mathrm{v},i}$ as in (21b), we obtain a closed-loop system equivalent to (22), which is clearly of the form (25). Moreover, EIP and $\bar{q}_i = q_i^*$ directly follow from Proposition 3 and Assumption 4. Finally, for $i \in \mathcal{L}_{\mathrm{VSP}}$, we fix $u_{\mathrm{v},i} = \bar{u}_{\mathrm{v},i} > 0$ and assign $u_{\mathrm{P},i}$ as in (15b). Then, the resulting closed-loop system is equivalent to (53) with the same EIP and equilibrium properties.

Next, we consider $i \in \mathcal{P}_{\mathrm{boost}}$, i.e., an arbitrary pipe in series with a booster pump. By combining the open-loop pipe model (4) with $u_{\mathrm{P},i}$ as in (10d), we can write the closed-loop dynamics as in (25), i.e.,

$$\underbrace{\frac{\mathrm{d}}{\mathrm{d}t}\begin{bmatrix} J_i q_i \\ J_{\mathrm{P},i}\chi_i \\ C_{\mathrm{P},i}\, p_{\mathrm{P},i} \\ Q_{\mathrm{I},i} r_i \end{bmatrix}}_{\dot{\hat{\boldsymbol{x}}}_i} = \underbrace{\begin{bmatrix} p_{\mathrm{P},i} - \lambda_i(q_i) \\ -R^{\mathrm{p}}_i \chi_i - (p_{\mathrm{P},i} - p^*_{\mathrm{P},i}) \\ \chi_i - r_i \\ (p_{\mathrm{P},i} - p^*_{\mathrm{P},i}) \end{bmatrix}}_{\hat{f}_i(\hat{\boldsymbol{x}}_i)} + \underbrace{\begin{bmatrix} 1 \\ 0 \\ 0 \\ 0 \end{bmatrix}}_{\hat{\boldsymbol{K}}_i} d_i \tag{56a}$$

$$z_i = \underbrace{\begin{bmatrix} \frac{1}{J_i} & 0 & 0 & 0 \end{bmatrix}}_{\hat{\boldsymbol{T}}_i} \hat{\boldsymbol{x}}_i \tag{56b}$$

with d_i as in (4). To show that (56) is EIP, we note that $\hat{H}_i$ is given by (26) with

$$\hat{\boldsymbol{Q}}_i = \operatorname{diag}^{-1}\big(J_i,\, J_{\mathrm{P},i},\, C_{\mathrm{P},i},\, Q_{\mathrm{I},i}\big). \tag{57}$$

The time derivative of $\hat{H}_i$ along the solutions of (56) satisfies

$$\dot{\hat{H}}_i = \nabla^\top \hat{H}_i \dot{\hat{x}}_i = -\hat{\psi}_i(\hat{x}_i) + (z_i - \bar{z}_i)(d_i - \bar{d}_i) \tag{58}$$

$$\hat{\psi}_i(\hat{\boldsymbol{x}}_i) = (q_i - \bar{q}_i)\big(\lambda_i(q_i) - \lambda_i(\bar{q}_i)\big) + R^{\mathrm{P}}_i(\chi_i - \bar{\chi}_i)^2 \tag{59}$$

where we have used the identity

$$\hat{\boldsymbol{K}}_i^\top \nabla \hat{H}_i = z_i - \bar{z}_i = q_i - \bar{q}_i = \hat{\boldsymbol{T}}_i(\hat{\boldsymbol{x}}_i - \bar{\hat{x}}_i).$$

As λ_i is strictly increasing and $R^{\mathrm{P}}_i > 0$, it follows that $\hat{\psi}_i(\hat{\boldsymbol{x}}_i) \geq 0$ and $\dot{\hat{H}}_i \leq (z_i - \bar{z}_i)(d_i - \bar{d}_i)$. Hence, (56) is EIP. Finally, observe that due to the integral action (10a), it holds for any feasible equilibrium value $\hat{\boldsymbol{x}}_i$ that $\bar{p}_{\mathrm{P},i} = p^*_{\mathrm{P},i}$.

The final type of actuated edges corresponds to mixing valves $i \in \mathcal{M}$. By combining the open-loop model (6) with $u_{\mathrm{v},i}$ as in (21b), we obtain a closed-loop system equivalent to (22), which is clearly of the form (25). Moreover, EIP and $\bar{q}_i = q_i^*$ directly follow from Proposition 3 and Assumption 4.

Finally, we consider pressure holding units $i \in \mathcal{H}$, which are the only actuated nodes. By combining the open-loop

model (8) with $u_{\mathrm{P},i}$ as in (10d), we obtain a closed-loop system equivalent to (11). Clearly, this system can be written as in (25). Moreover, EIP and $\bar{p}_{\mathrm{P},i} = p^*_{\mathrm{P},i}$ follow directly from Proposition 1.

Appendix E
Proof of Lemma 2

For any pipe $i \in \mathcal{P} \setminus \mathcal{P}_{\mathrm{boost}}$ without booster pump, we use the open-loop model (4) and set $u_{\mathrm{P},i} = 0$ to obtain a model of the form (25) with

$$\frac{\mathrm{d}}{\mathrm{d}t} \underbrace{J_i q_i}_{\hat{x}_i} = \underbrace{-\lambda_i(q_i)}_{\hat{f}_i(\hat{x}_i)} + \underbrace{[1]}_{\hat{K}_i} d_i \tag{60a}$$

$$z_i = q_i = \underbrace{\begin{bmatrix} 1 \\ \overline{J_i} \end{bmatrix}}_{\hat{T}_i} \hat{x}_i \tag{60b}$$

where d_i is as in (4). EIP of (60) follows directly by using $\hat{H}_i$ in (26) as storage function with $\hat{Q}_i = (1/J_i)$ and noting that

$$\dot{\hat{H}}_i = -\hat{\psi}_i(\hat{x}_i) + (z_i - \bar{z}_i)(d_i - \bar{d}_i) \tag{61a}$$

$$\hat{\psi}_i(\hat{x}_i) = (q_i - \bar{q}_i)(\lambda_i(q_i) - \lambda_i(\bar{q}_i)) \geq 0. \tag{61b}$$

Writing the model (9) of any capacitive node $i \in \mathcal{C}$ as in (25) is trivial. Furthermore, EIP of the system (9) follows directly by using $\hat{H}_i$ in (26) as a storage function with $\hat{Q}_i = (1/C_i)$ and noting that

$$\dot{\hat{H}}_i(\hat{x}_i) = (z_i - \bar{z}_i)(d_i - \bar{d}_i). \tag{62}$$

Appendix F
Proof of Theorem 1

Let $(\bar{\hat{x}}_{\mathcal{E}}, \bar{\hat{x}}_{\Delta})$ denote a feasible equilibrium of the closed-loop system (32). Due to Lemma 1, this equilibrium is such that each bullet point in Problem 1 is fulfilled. Then, consider the Lyapunov function candidate

$$V(\hat{\boldsymbol{x}}_{\mathcal{E}}, \hat{\boldsymbol{x}}_{\Delta}) = \sum_{i \in \mathcal{E} \cup \Delta} \hat{H}_i(\hat{x}_i) \tag{63}$$

where each $\hat{H}_i$ is defined in Lemma 1 or 2. Note that $V(\hat{\boldsymbol{x}}_{\mathcal{E}}, \hat{\boldsymbol{x}}_{\Delta}) > 0$ for all $(\hat{\boldsymbol{x}}_{\mathcal{E}}, \hat{\boldsymbol{x}}_{\Delta}) \neq (\bar{\hat{x}}_{\mathcal{E}}, \bar{\hat{x}}_{\Delta})$ and $V(\bar{\hat{x}}_{\mathcal{E}}, \bar{\hat{x}}_{\Delta}) = 0$. Via direct computations, it can be shown that the time derivative of V along the solutions of (32) on the invariant set $\mathbb{M}$ in (33) is given by

$$\begin{aligned} \dot{V}(\hat{\boldsymbol{x}}_{\mathcal{E}}, \hat{\boldsymbol{x}}_{\Delta}) &= \sum_{i \in \mathcal{E} \cup \Delta} \nabla \hat{H}_i^{\top}(\hat{x}_i) \dot{\hat{x}}_i \\ &= \sum_{i \in \mathcal{E} \cup \Delta} \nabla \hat{H}_i^{\top}(\hat{x}_i)(\hat{f}_i(\hat{x}_i) - \hat{f}_i(\bar{\hat{x}}_i)) \end{aligned} \tag{64}$$

where we have implicitly used Lemma 3 to cancel out cross terms. Stability of $(\bar{\hat{x}}_{\mathcal{E}}, \bar{\hat{x}}_{\Delta})$ follows directly from (64), as its right-hand side is upper bounded by zero according to the EIP properties established in Lemmas 1 and 2.

We move on to show that $(\bar{\hat{x}}_{\mathcal{E}}, \bar{\hat{x}}_{\Delta})$ is, in fact, asymptotically stable. Considering LaSalle's invariance principle, it is sufficient to show that $(\bar{\hat{x}}_{\mathcal{E}}, \bar{\hat{x}}_{\Delta})$ is the largest invariant set of (32) where $\dot{V}$ is zero. As a first step, we characterize the conditions under which $\dot{V}(\hat{\boldsymbol{x}}) = 0$. For that we split the summands in the right-hand side of (64) as follows.

First, from the proof of Lemma 1, we have that

$$\sum_{i \in \mathcal{D}} \nabla \hat{H}_i^{\top}(\hat{x}_i)(\hat{f}_i(\hat{x}_i) - \hat{f}_i(\bar{\hat{x}}_i)) = -\sum_{i \in \mathcal{D}} \hat{\psi}_i(\hat{x}_i) \tag{65}$$

where $\hat{\psi}_i$ is given in (48), (52), and (55) for i in $\mathcal{D}_{\mathrm{form}}$, $\mathcal{D}_{\mathrm{valve}}$, and $\mathcal{D}_{\mathrm{VSP}}$, respectively. For $i \in \mathcal{D}_{\mathrm{form}}$, the mononoticities of λ_i and $\hat{\mu}_i$, and the condition $\bar{u}_{\mathrm{v},i} > 0$ (see Assumption 2), imply that $\hat{\psi}_i(\hat{x}_i) = 0$ if and only if

$$\hat{x}_i \in \Xi_i = \{\hat{x}_i : \ q_i = \bar{q}_i, \ \ \chi_i = \bar{\chi}_i = 0\}. \tag{66}$$

For $i \in \mathcal{D}_{\mathrm{valve}}$, the monotonicity of λ_i in combination with Assumptions 2 and 4 implies that $\hat{\psi}_i(\hat{x}_i) = 0$ if and only if

$$\hat{x}_i \in \Xi_i = \{\hat{x}_i : \ q_i = \bar{q}_i = q_i^*, \ \ \chi_i = \bar{\chi}_i = 0\}. \tag{67}$$

For $i \in \mathcal{D}_{\mathrm{VSP}}$, the monotonicities of λ_i and $\hat{\mu}_i$, and the condition $\bar{u}_{\mathrm{v},i} > 0$ (see again Assumptions 2 and 4), imply that $\hat{\psi}_i(\hat{x}_i) = 0$ if and only if

$$\hat{x}_i \in \Xi_i = \{\hat{x}_i : \ q_i = \bar{q}_i = q_i^*, \ \ q_{\mathrm{P},i} = \bar{q}_{\mathrm{P},i} = q_i^*\}. \tag{68}$$

Following an analogous reasoning for the set of consumers $\mathcal{L}$, we have from Lemma 1 that

$$\sum_{i \in \mathcal{L}} \nabla \hat{H}_i^{\top}(\hat{x}_i)(\hat{f}_i(\hat{x}_i) - \hat{f}_i(\bar{\hat{x}}_i)) = -\sum_{i \in \mathcal{L}} \hat{\psi}_i(\hat{x}_i) \tag{69}$$

with $\hat{\psi}_i = \hat{\psi}_k$ as in (52) for $i \in \mathcal{L}_{\mathrm{boost}}$ and $k \in \mathcal{D}_{\mathrm{valve}}$; $\hat{\psi}_i = \psi_i^{\mathrm{v}}$ as in (44) for $i \in \mathcal{L}_{\mathrm{valve}}$; and $\hat{\psi}_i = \hat{\psi}_k$ as in (55) for $i \in \mathcal{L}_{\mathrm{VSP}}$ and $k \in \mathcal{D}_{\mathrm{VSP}}$ Then, $\hat{\psi}_i(\hat{x}_i) = 0$ for $i \in \mathcal{L}_{\mathrm{boost}}$ if and only if

$$\hat{x}_i \in \Xi_i = \{\hat{x}_i : \ q_i = \bar{q}_i = q_i^*, \ \ \chi_i = \bar{\chi}_i = 0\} \tag{70}$$

$\hat{\psi}_i(\hat{x}_i) = 0$ for $i \in \mathcal{L}_{\mathrm{valve}}$ if and only if

$$\hat{x}_i \in \Xi_i = \{\hat{x}_i : \ q_i = \bar{q}_i = q_i^*\} \tag{71}$$

and $\hat{\psi}_i(\hat{x}_i) = 0$ for $i \in \mathcal{L}_{\mathrm{VSP}}$ if and only if

$$\hat{x}_i \in \Xi_i = \{\hat{x}_i : \ q_i = \bar{q}_i = q_i^*, \ \ q_{\mathrm{P},i} = \bar{q}_{\mathrm{P},i} = q_i^*\}. \tag{72}$$

Moving on to the pipes with booster pumps $\mathcal{P}_{\mathrm{boost}}$, it holds due to Lemma 1 that

$$\sum_{i \in \mathcal{P}_{\mathrm{boost}}} \nabla \hat{H}_i^{\top}(\hat{x}_i)(\hat{f}_i(\hat{x}_i) - \hat{f}_i(\bar{\hat{x}}_i)) = -\sum_{i \in \mathcal{P}_{\mathrm{boost}}} \hat{\psi}_i(\hat{x}_i) \tag{73}$$

with $\hat{\psi}_i$ as in (59). Then, it holds that $\hat{\psi}_i(\hat{x}_i) = 0$ for $i \in \mathcal{P}_{\mathrm{boost}}$ if and only if

$$\hat{x}_i \in \Xi_i = \{\hat{x}_i : \ q_i = \bar{q}_i, \ \ \chi_i = \bar{\chi}_i = 0\}. \tag{74}$$

Next, we consider the set of mixing valves $\mathcal{M}$. Due to Lemma 1, it holds that

$$\sum_{i \in \mathcal{M}} \nabla \hat{H}_i^{\top}(\hat{x}_i)(\hat{f}_i(\hat{x}_i) - \hat{f}_i(\bar{\hat{x}}_i)) = -\sum_{i \in \mathcal{M}} \hat{\psi}_i(\hat{x}_i) \tag{75}$$

with $\hat{\psi}_i = \psi_i^{\mathrm{v}}$ as in (44). Then, considering Assumption 4, it holds that $\hat{\psi}_i(\hat{x}_i) = 0$ for $i \in \mathcal{M}$ if and only if

$$\hat{x}_i \in \Xi_i = \{\hat{x}_i : \ q_i = \bar{q}_i = q_i^*\}. \tag{76}$$

Moving on to the set of pipes without booster pumps $\mathcal{P} \setminus \mathcal{P}_{\text{boost}}$, we get from Lemma 2 and its proof that

$$\sum_{i\in\mathcal{P}\setminus\mathcal{P}_{\text{boost}}} \nabla \hat{H}_i^\top(\hat{\boldsymbol{x}}_i)\big(\hat{\boldsymbol{f}}_i(\hat{\boldsymbol{x}}_i) - \hat{\boldsymbol{f}}_i(\bar{\hat{\boldsymbol{x}}}_i)\big) = -\sum_{i\in\mathcal{P}\setminus\mathcal{P}_{\text{boost}}} \hat{\psi}_i(\hat{\boldsymbol{x}}_i) \tag{77}$$

with $\hat{\psi}_i$ as in (61). Then, $\hat{\psi}_i(\hat{\boldsymbol{x}}_i) = 0$ for $i \in \mathcal{P} \setminus \mathcal{P}_{\text{boost}}$ if and only if

$$\hat{\boldsymbol{x}}_i \in \Xi_i = \big\{\hat{\boldsymbol{x}}_i :\ q_i = \bar{q}_i\big\}. \tag{78}$$

For the set of pressure holding units $\mathcal{H}$ [in closed loop with (10)], we have from Lemma 1 (and Proposition 1) that

$$\sum_{i\in\mathcal{H}} \nabla \hat{H}_i^\top(\hat{\boldsymbol{x}}_i)\big(\hat{\boldsymbol{f}}_i(\hat{\boldsymbol{x}}_i) - \hat{\boldsymbol{f}}_i(\bar{\hat{\boldsymbol{x}}}_i)\big) = -\sum_{i\in\mathcal{H}} \hat{\psi}_i(\hat{\boldsymbol{x}}_i) \tag{79}$$

with $\hat{\psi}_i = \psi_i^{\text{p}}$ as in (38). Then, $\hat{\psi}_i(\hat{\boldsymbol{x}}_i) = 0$ for $i \in \mathcal{H}$ if and only if

$$\hat{\boldsymbol{x}}_i \in \Xi_i = \big\{\hat{\boldsymbol{x}}_i :\ \chi_i = \bar{\chi}_i = 0\big\}. \tag{80}$$

For the set of capacitive nodes $\mathcal{C}$, it holds from the proof of Lemma 2 that

$$\sum_{i\in\mathcal{C}} \nabla \hat{H}_i^\top(\hat{\boldsymbol{x}}_i)\big(\hat{\boldsymbol{f}}_i(\hat{\boldsymbol{x}}_i) - \hat{\boldsymbol{f}}_i(\bar{\hat{\boldsymbol{x}}}_i)\big) = 0. \tag{81}$$

Considering these developments, its possible to characterize the condition $\dot{V}(\hat{\boldsymbol{x}}_{\mathcal{E}}, \hat{\boldsymbol{x}}_{\Delta}) = 0$ as follows:

$$\dot{V}\big(\hat{\boldsymbol{x}}\big) = 0 \Leftrightarrow \hat{\boldsymbol{x}} \in \Xi$$
$$\Xi = \big\{\hat{\boldsymbol{x}} :\ \hat{x}_i \in \Xi_i,\ \forall i \in \mathcal{E} \cup \Delta\big\}.$$

To show asymptotic stability of $(\bar{\hat{\boldsymbol{x}}}_{\mathcal{E}}, \bar{\hat{\boldsymbol{x}}}_{\Delta})$, let $(\hat{\boldsymbol{x}}_{\mathcal{E}}, \hat{\boldsymbol{x}}_{\Delta}) \in \Xi$ be any solution of (32) in the manifold $\mathbb{M}$ that remains in Ξ for all time. Then, we directly have that $q_i = \bar{q}_i$ for all $i \in \mathcal{E}$. Next, we show that $q_i = \bar{q}_i$ for all $i \in \mathcal{E}$ implies $p_j = \bar{p}_j$ for all $j \in \Delta$ and that eventually these two conditions imply that $r_k = \bar{r}_k$ for all $k \in \mathcal{D} \cup \mathcal{L} \cup \mathcal{P}_{\text{boost}} \cup \mathcal{M} \cup \mathcal{H}$ and, hence, that $(\hat{\boldsymbol{x}}_{\mathcal{E}}, \hat{\boldsymbol{x}}_{\Delta}) = (\bar{\hat{\boldsymbol{x}}}_{\mathcal{E}}, \bar{\hat{\boldsymbol{x}}}_{\Delta})$.

From the dynamics (9) of any capacitive node $j \in \mathcal{C}$, we have that if $q_i = \bar{q}_i$ for all $i \in \mathcal{E}$, then $\dot{p}_j = 0$ for all time ($\sum_{i\in\mathcal{I}_j} \bar{q}_i = 0$ due to volume balance). From the closed-loop dynamics (11) of any pressure holding unit $j \in \mathcal{H}$, the condition $q_i = \bar{q}_i$ for all $i \in \mathcal{E}$ together with $\chi_j = 0$ leads to $p_{\text{P},j} = \bar{p}_{\text{P},j} = p^*_{\text{P},j}$. This means that if $(\hat{\boldsymbol{x}}_{\mathcal{E}}, \hat{\boldsymbol{x}}_{\Delta}) \in \mathbb{M} \cap \Xi$ for all time, both $q_i = \bar{q}_i$ for all $i \in \mathcal{E}$ and $p_j = \bar{p}_j$ for all $j \in \Delta$. A consequence of this is that $r_i = \bar{r}_i$ for any $i \in \mathcal{D} \cup \mathcal{L} \cup \mathcal{P}_{\text{boost}} \cup \mathcal{M} \cup \mathcal{H}$. Indeed, see, on the one hand, the definition of the pumps and valves controllers (Propositions 1–3) that $\dot{r}_i$ would be zero. On the other hand, since r_i enters linearly in the dynamics of the—now at equilibrium variables χ_i, $q_{\text{P},i}$, or q_i, of the respective pumps and valves dynamics—then $r_i = \bar{r}_i$. Therefore, $(\bar{\hat{\boldsymbol{x}}}_{\mathcal{E}}, \bar{\hat{\boldsymbol{x}}}_{\Delta})$ is the largest invariant set of the overall closed-loop DHN dynamics contained in Ξ. By LaSalle's invariance principle, $\hat{x}$ is an asymptotically stable equilibrium point.

ACKNOWLEDGMENT

An extended version of this article with more background information and technical details can be found in [1].

REFERENCES

[1] F. Strehle, J. E. Machado, M. Cucuzzella, A. J. Malan, J. M. A. Scherpen, and S. Hohmann, "A unifying passivity-based framework for pressure and volume flow rate control in district heating networks," 2023, *arXiv:2305.12139*.

[2] H. Lund et al., "4th generation district heating (4GDH): Integrating smart thermal grids into future sustainable energy systems," *Energy*, vol. 68, pp. 1–11, Apr. 2014.

[3] A. Vandermeulen, B. van der Heijde, and L. Helsen, "Controlling district heating and cooling networks to unlock flexibility: A review," *Energy*, vol. 151, pp. 103–115, May 2018.

[4] N. N. Novitsky et al., "Smarter smart district heating," *Proc. IEEE*, vol. 108, no. 9, pp. 1596–1611, Sep. 2020.

[5] H. Wang, H. Wang, and T. Zhu, "A new hydraulic regulation method on district heating system with distributed variable-speed pumps," *Energy Convers. Manage.*, vol. 147, pp. 174–189, Sep. 2017.

[6] Z. Pan, Q. Guo, and H. Sun, "Interactions of district electricity and heating systems considering time-scale characteristics based on quasi-steady multi-energy flow," *Appl. Energy*, vol. 167, pp. 230–243, Apr. 2016.

[7] T. Nussbaumer, S. Thalmann, A. Jenni, and J. Ködel, *Handbook on Planning of District Heating Networks*. Bern, Switzerland: QM Fernwärme and EnergieSchweiz, 2020.

[8] F. Strehle, J. Vieth, M. Pfeifer, and S. Hohmann, "Passivity-based stability analysis of hydraulic equilibria in 4th generation district heating networks," *IFAC-PapersOnLine*, vol. 54, no. 19, pp. 261–266, 2021.

[9] A. Yan, J. Zhao, Q. An, Y. Zhao, H. Li, and Y. J. Huang, "Hydraulic performance of a new district heating systems with distributed variable speed pumps," *Appl. Energy*, vol. 112, pp. 876–885, Dec. 2013.

[10] E. Gong, N. Wang, S. You, Y. Wang, H. Zhang, and S. Wei, "Optimal operation of novel hybrid district heating system driven by central and distributed variable speed pumps," *Energy Convers. Manage.*, vol. 196, pp. 211–226, Sep. 2019.

[11] M. Köfinger, D. Basciotti, and R.-R. Schmidt, "Reduction of return temperatures in urban district heating systems by the implementation of energy-cascades," *Energy Proc.*, vol. 116, pp. 438–451, Jun. 2017.

[12] A. Volkova et al., "Energy cascade connection of a low-temperature district heating network to the return line of a high-temperature district heating network," *Energy*, vol. 198, May 2020, Art. no. 117304.

[13] A. Volkova et al., "Cascade sub-low temperature district heating networks in existing district heating systems," *Smart Energy*, vol. 5, Feb. 2022, Art. no. 100064.

[14] C. De Persis and C. S. Kallesoe, "Pressure regulation in nonlinear hydraulic networks by positive and quantized controls," *IEEE Trans. Control Syst. Technol.*, vol. 19, no. 6, pp. 1371–1383, Nov. 2011.

[15] B. van der Heijde et al., "Dynamic equation-based thermo-hydraulic pipe model for district heating and cooling systems," *Energy Convers. Manage.*, vol. 151, pp. 158–169, Nov. 2017.

[16] J. Mohring, D. Linn, M. Eimer, M. Rein, and N. Siedow, "District heating networks–dynamic simulation and optimal operation," in *Mathematical Modeling, Simulation and Optimization for Power Engineering and Management*. Cham, Switzerland: Springer, 2021, pp. 303–325.

[17] T. Sommer, S. Mennel, and M. Sulzer, "Lowering the pressure in district heating and cooling networks by alternating the connection of the expansion vessel," *Energy*, vol. 172, pp. 991–996, Apr. 2019.

[18] R. Ortega and E. García-Canseco, "Interconnection and damping assignment passivity-based control: A survey," *Eur. J. Control*, vol. 10, no. 5, pp. 432–450, Jan. 2004.

[19] A. Donaire and S. Junco, "On the addition of integral action to port-controlled Hamiltonian systems," *Automatica*, vol. 45, no. 8, pp. 1910–1916, Aug. 2009.

[20] P. Monshizadeh, J. E. Machado, R. Ortega, and A. van der Schaft, "Power-controlled Hamiltonian systems: Application to electrical systems with constant power loads," *Automatica*, vol. 109, Nov. 2019, Art. no. 108527.

[21] J. E. Machado, M. Cucuzzella, N. Pronk, and J. M. A. Scherpen, "Adaptive control for flow and volume regulation in multi-producer district heating systems," *IEEE Control Syst. Lett.*, vol. 6, pp. 794–799, 2022.

[22] T. N. Jensen, "Plug and play control of hydraulic networks," Ph.D. dissertation, Dept. Electron. Syst., Automat. Control, Aalborg Univ., Copenhagen, Denmark, 2012.

[23] C. De Persis, T. N. Jensen, R. Ortega, and R. Wisniewski, "Output regulation of large-scale hydraulic networks," *IEEE Trans. Control Syst. Technol.*, vol. 22, no. 1, pp. 238–245, Jan. 2014.

[24] T. Scholten, S. Trip, and C. De Persis, "Pressure regulation in large scale hydraulic networks with input constraints," *IFAC-PapersOnLine*, vol. 50, no. 1, pp. 5367–5372, 2017.
[25] S.-A. Hauschild et al., "Port-Hamiltonian modeling of district heating networks," in *Progress in Differential-Algebraic Equations II* (Differential-Algebraic Equations Forum). Cham, Switzerland: Springer, 2020, pp. 333–355.
[26] F. Strehle, J. E. Machado, M. Cucuzzella, A. J. Malan, J. M. A. Scherpen, and S. Hohmann, "Port-Hamiltonian modeling of hydraulics in 4th generation district heating networks," in *Proc. IEEE 61st Conf. Decis. Control (CDC)*, Dec. 2022, pp. 1182–1189.
[27] R. Perryman, J. A. Taylor, and B. Karney, "Port-Hamiltonian based control of water distribution networks," *Syst. Control Lett.*, vol. 170, Dec. 2022, Art. no. 105402.
[28] F. Goppelt, T. Hieninger, and R. Schmidt-Vollus, "Modeling centrifugal pump systems from a system-theoretical point of view," in *Proc. 18th Int. Conf. Mechatronics Mechatronika (ME)*, Dec. 2018, pp. 1–8.
[29] C. S. Kallesoe, V. Cocquempot, and R. Izadi-Zamanabadi, "Model based fault detection in a centrifugal pump application," *IEEE Trans. Control Syst. Technol.*, vol. 14, no. 2, pp. 204–215, Mar. 2006.
[30] H. Li et al., *Future Low Temperature District Heating Design Guidebook: Final Report of IEA DHC Annex TS1. Low Temperature District Heating for Future Energy Systems*. Paris, France: International Energy Agency, 2017.
[31] M. Chertkov and N. N. Novitsky, "Thermal transients in district heating systems," *Energy*, vol. 184, pp. 22–33, Oct. 2019.
[32] A. van der Schaft, *L2-Gain and Passivity Techniques in Nonlinear Control*, 3rd ed. Cham, Switzerland: Springer, 2017.
[33] Y. Wang, S. You, H. Zhang, W. Zheng, X. Zheng, and Q. Miao, "Hydraulic performance optimization of meshed district heating network with multiple heat sources," *Energy*, vol. 126, pp. 603–621, May 2017.
[34] H. Boysen and J. E. Thorsen, *How to Avoid Pressure Oscillations in District Heating Systems*. Nordborg, Denmark: Danfoss A/S, Nordborg, 2003.
[35] J. E. Machado, M. Cucuzzella, and J. M. A. Scherpen, "Modeling and passivity properties of multi-producer district heating systems," *Automatica*, vol. 142, Aug. 2022, Art. no. 110397.
[36] G. Lennermo, P. Lauenburg, and S. Werner, "Control of decentralised solar district heating," *Sol. Energy*, vol. 179, pp. 307–315, Feb. 2019.
[37] N. Lamaison, R. Bavière, D. Cheze, and C. Paulus, "A multi-criteria analysis of bidirectional solar district heating substation architecture," in *Proc. SWC/SHC*, Oct. 2017, pp. 1–11.
[38] B. Stræde, *Pressure Oscillation in District Heating Installations*. Nordborg, Denmark: Danfoss A/S, 1995.
[39] S. Buffa, M. H. Fouladfar, G. Franchini, I. L. Gabarre, and M. A. Chicote, "Advanced control and fault detection strategies for district heating and cooling systems—A review," *Appl. Sci.*, vol. 11, no. 1, p. 455, Jan. 2021.
[40] *Pump Control / System Automation*, KSB Aktiengesellschaft, Frankenthal, Germany, 2006.
[41] G. Lennermo, P. Lauenburg, and L. Brand, "Decentralised heat supply in district heating systems: Implications of varying differential pressure," in *Proc. From 14th Int. Symp. District Heating Cooling*, 2014.
[42] R. Krug, V. Mehrmann, and M. Schmidt, "Nonlinear optimization of district heating networks," *Optim. Eng.*, vol. 22, no. 2, pp. 783–819, Jun. 2021.
[43] V. D. Stevanovic, S. Prica, B. Maslovaric, B. Zivkovic, and S. Nikodijevic, "Efficient numerical method for district heating system hydraulics," *Energy Convers. Manage.*, vol. 48, no. 5, pp. 1536–1543, May 2007.
[44] M. Arcak, C. Meissen, and A. Packard, *Networks of Dissipative Systems: Compositional Certification of Stability, Performance, and Safety* (SpringerBriefs in Control, Automation and Robotics). New York, NY, USA: Springer, 2016.
[45] F. Strehle, P. Nahata, A. J. Malan, S. Hohmann, and G. Ferrari-Trecate, "A unified passivity-based framework for control of modular islanded AC microgrids," *IEEE Trans. Control Syst. Technol.*, vol. 30, no. 5, pp. 1960–1976, Sep. 2022.
[46] P. Nahata, R. Soloperto, M. Tucci, A. Martinelli, and G. Ferrari-Trecate, "A passivity-based approach to voltage stabilization in DC microgrids with ZIP loads," *Automatica*, vol. 113, Mar. 2020, Art. no. 108770.
[47] D. A. Harney, T. K. Mills, and N. L. Book, "Numerical evaluation of the stability of stationary points of index-2 differential-algebraic equations: Applications to reactive flash and reactive distillation systems," *Comput. Chem. Eng.*, vol. 49, pp. 61–69, Feb. 2013.
[48] U. Miekkala, "Graph properties for splitting with grounded Laplacian matrices," *BIT*, vol. 33, no. 3, pp. 485–495, Sep. 1993.

Felix Strehle received the B.Sc. and M.Sc. degrees in electrical engineering and information technology and the Ph.D. degree in control engineering from the Karlsruhe Institute of Technology (KIT), Karlsruhe, Germany, in 2015, 2017, and 2024, respectively.

Since June 2022, he has been leading the research group on networked multienergy systems at the Institute of Control Systems (IRS), KIT. His main research interests are centered around energy-based modeling and decentralized, passivity-based control, and stability with application to networked multi-energy systems, such as power systems, microgrids, district heating networks, gas networks, and integrated combinations thereof.

Juan E. Machado received the B.Sc. degree in electromechanics from the Technological Institute of La Paz (ITLP), La Paz, Mexico, in 2012, the M.Sc. degree in applied mathematics from the Center for Research in Mathematics (CIMAT), Guanajuato, Mexico, in 2015, and the Ph.D. degree in automatic control from Paris-Saclay University, Gif-sur-Yvette, France, in 2019.

From January 2020 to June 2023, he was a Post-Doctoral Researcher at the Faculty of Science and Engineering, University of Groningen, Groningen, The Netherlands. Since July 2023, he has been with the Chair of Control Systems and Network Control Technology, Faculty of Mechanical Engineering, Electrical and Energy Systems, Brandenburg University of Technology (BTU), Cottbus, Germany, where he is currently a Junior Research Group Leader of the Young Investigator Group (YIG) "Distributed Control and Operation of Integrated Energy Systems," which is part of the Project "Control Systems and Cyber Security Lab (COSYS Lab)" of the Energy Innovation Center (EIZ). His research interests are within the analysis and control of nonlinear and networked systems, with a strong emphasis on electric and heat grids.

Michele Cucuzzella (Member, IEEE) received the M.Sc. degree (Hons.) in electrical engineering and the Ph.D. degree in systems and control from the University of Pavia, Pavia, Italy, in 2014 and 2018, respectively.

From 2017 to 2020, he was a Post-Doctoral Researcher at the University of Groningen (UG), Groningen, The Netherlands. He then joined the University of Pavia as an Assistant Professor, and in 2024, he moved to the Engineering and Technology Institute Groningen, Faculty of Science and Engineering, UG, as an Associate Professor. He is also a Visiting Associate Professor at Hiroshima University, Higashihiroshima, Japan. He has coauthored the book *Advanced and Optimization Based Sliding Mode Control: Theory and Applications* (SIAM, 2019). His research activities are mainly in the area of nonlinear control with application to the energy domain and smart complex systems.

Dr. Cucuzzella is a member of the European Control Association (EUCA) Conference Editorial Board and the IEEE CSS Technology Conferences Editorial Board. He received the Certificate of Outstanding Service as a reviewer of the IEEE CONTROL SYSTEMS LETTERS in 2019. He also received the 2020 IEEE TRANSACTIONS ON CONTROL SYSTEMS TECHNOLOGY Outstanding Paper Award, the IEEE Italy Section Award for the best Ph.D. thesis on new technological challenges in energy and industry, and the SIDRA Award for the best Ph.D. thesis in the field of systems and control engineering. He was also the Finalist for the EECI Award for the best Ph.D. thesis in Europe in the field of control for complex and heterogeneous systems and for the IEEE CSS Italy Best Young Paper Award. He has been serving as an Associate Editor for the *European Journal of Control* since 2022.

Albertus Johannes Malan received the B.Eng. degree in electronic engineering from the University of Pretoria, Pretoria, South Africa, in 2015, and the M.Sc. degree in electrical engineering and information technology from the Karlsruhe Institute of Technology (KIT), Karlsruhe, Germany, in 2019, where he is currently pursuing the Ph.D. degree in networked multienergy systems with the Institute of Control Systems (IRS).

He works as a Research Associate at IRS, KIT. His research interests include multiagent systems, passivity-based stability, and the control of energy networks.

Sören Hohmann (Member, IEEE) received the Diploma and Ph.D. degrees in electrical engineering from the University of Karlsruhe, Karlsruhe, Germany, in 1997 and 2002, respectively, after studying electrical engineering jointly at the Technische Universität Braunschweig, Brunswick, Germany, the University of Karlsruhe, and the École Nationale Supérieure d'Électricité et de Mécanique, Nancy, France.

Afterwards, until 2010, he worked in the industry for BMW, Munich, Germany, where his last position was the head of the predevelopment and series development of active safety systems. He is currently the Head of the Institute of Control Systems (IRS), Karlsruhe Institute of Technology (KIT), Karlsruhe, and the Director's Board Member of the Research Center for Information Technology(FZI), Karlsruhe. His research interests are cooperative control, networked multienergy systems, and system guarantees by design.

Jacquelien M. A. Scherpen (Fellow, IEEE) received the M.Sc. and Ph.D. degrees from the University of Twente, Enschede, The Netherlands, in 1990 and 1994, respectively.

She then joined the Delft University of Technology, Delft, The Netherlands, and in 2006, she moved to the Engineering and Technology Institute Groningen (ENTEG), Faculty of Science and Engineering, University of Groningen (UG), Groningen, The Netherlands, where she was the Scientific Director of ENTEG and the Director of engineering. She is currently the Rector Magnificus of UG. Furthermore, she has been the Captain of Science of the Dutch Top Sector High Tech Systems and Materials (HTSM). She has held various visiting research positions at the University of Tokyo, Tokyo, Japan; Kyoto University, Kyoto, Japan; Old Dominion University, Norfolk, VA, USA; the Université de Compiègne, Compiègne, France; and Supélec, Gif-sur-Yvette, France. Her current research interests include model reduction methods for networks, nonlinear model reduction methods, nonlinear control methods, modeling and control of physical systems with applications to electrical circuits, electromechanical systems, mechanical systems, smart energy networks, and distributed optimal control for smart grids.

Dr. Scherpen received the 2017–2020 Automatica Best Paper Prize. In 2019, she received the Royal Distinction as Knight in the Order of the Netherlands Lion. In 2023, she was awarded the Prince Friso Prize for Engineer of the Year in The Netherlands. She has been active at the International Federation of Automatic Control (IFAC) and the IEEE Control Systems Society. She was the President of the European Control Association (EUCA) and has chaired the SIAM Activity Group on Control and Systems Theory. She has been on the Editorial Board of a few international journals among which are IEEE TRANSACTIONS ON AUTOMATIC CONTROL and the *International Journal of Robust and Nonlinear Control*.

Open Access funding provided by 'Università degli Studi di Pavia' within the CRUI CARE Agreement